The core of GIScience
a process-based approach

ITC Educational textbook series

UNIVERSITY OF TWENTE

FACULTY OF GEO-INFORMATION SCIENCE AND EARTH OBSERVATION

ITC

Chapter 11

Data integration

Dinand Alkema
Wietske Bijker
Ali Sharifi
Zoltan Vekerdy
Wouter Verhoef

11.1 Introduction

Processes on the planet Earth are complex phenomena that are taking place in space and in time, i.e. in four dimensions. In many of these processes, differences in one dimension (e.g. height above the geoid) can be disregarded, so that two spatial dimensions and the dimension time remain. Despite this simplification, the physical description of the phenomena remains a difficult task. To better understand the processes it often helps if the same geographic region is viewed repeatedly and, if possible, also from different directions and in different wavelength regions. Integration of data from a variety of sources can be a means to retrieving information about processes that would otherwise remain undetected.

Examples of important Earth system processes are:

- Volcanism, earthquakes, plate tectonics
- Ocean currents
- Climate
- Weather
- The living planet (biosphere, agriculture)
- Human activities (urbanization).

Data integration, as the term specifies, concerns the combination and further integration of spatial data. Such a combination may seem at a glance to be simple, but there are various important and challenging issues around it. Indeed, we have seen in earlier chapters that the combination of remote sensing data is not at all trivial. Even if the

images come from geostationary satellites focusing at a single area of land, overlaying these images is still a skilled—although not very difficult—operation. Ground control points can play an essential role in this.

After the overlaying, integration then really concerns the combination of the different wavelength bands, times of observation and, possibly, viewing directions. In addition, the combination of different GIS layers may not be straightforward. Only if GIS layers have the same scale and represent comparable layers of information can overlaying be done sensibly, leading to a possible integration of the information on those layers. An even more challenging case is the combination of a vector layer with an image. For this, the same scale should apply, i.e. a common platform should be decided upon and both sources of data should be made available on this platform so that the overlaying step can be performed. Even then, full integration, i.e. the combination of the information in the two layers, demands that several steps be followed very carefully and close attention must be paid to issues of data quality. Combining layers and images becomes increasingly challenging as the data become more and more complicated. Combining, for example, LIDAR data obtained from an oblique point of view with data from other sources can be done, but usually mathematical transformations have to be applied. Similarly, the combination of data from active sensors with that from passive sensors, of field data with remote sensing data or field data with GIS layers are all activities that require a serious attention throughout.

In the past, much attention was paid to the activities of overlaying and data integration and this is currently still the case. Terms that one typically comes across in this area are conflation, of GIS layers, image fusion, of remote sensing images and registration. Conflation is a somewhat older concept that defines a range of activities that allow one to combine vector layers. Image fusion has had its roots within the ITC research notably by Pohl and van Genderen [92] and is now being further developed throughout the world. Image fusion is the process of combining relevant information from two or more images into a single image. The resulting image will be more informative than any of the input images as it can have complementary spatial and spectral resolution characteristics. In particular the combination of a high spatial and a high spectral resolution image into a single image can be successful. We distinguish fusion at the pixel level, from fusion at the segment level towards fusion at the object level. Image fusion at the pixel level allows the integration of images with each other, but also of an image with other information sources, such as a digital elevation model with images. At the segment level, hence after segmentation of the image, it allows integration with GIS layers. At the object level, hence after a classification, we can also speak about information fusion. Research at this level is still going on. Registration is a term referring to the combination of Earth observation and GIS layers. It is the process of transforming different sets of data into one coordinate system. Data may be multiple images, multiple GIS layers, images from different sensors, from different times, or from different viewpoints. It is used in compiling and analyzing satellite images. Registration is necessary in order to be able to compare or integrate the data obtained from these different measurements and some of it has been dealt with in Chapter 3.

As the focus of this chapter is data integration, it is assumed that the issue of overlaying has been solved, so we can then concentrate our attention on the combination of different layers of information in such a way that new, meaningful information is generated. In this sense, integration is close to modelling, although, as can be seen below, there are some clear distinctions between the two. The *multi* concept will also be introduced as a generic term for the integration of various images at various scales.

Data integration brings with it several issues that play a role in the processing of the data. The most important are:

- data models (raster, vector, TIN, etc.)
- data conversion
- resampling and (dis)aggregation
- gap filling and interpolation
- spectral, angular and temporal effects
- change detection
- visualization techniques
- data assimilation in process models
- multi-sensor approaches.

In this chapter, first a distinction is made between process models and observation models, and it is shown how both types of model can be used together to retrieve more and better information. Next,the *multi* concept in remote sensing is introduced. Data from multiple sources can be integrated to derive more geospatial information of higher quality. Other subjects covered in the chapter are spatial, temporal and spectral scales, and the data conversion issues that arise from data integration. Special attention is paid to change detection techniques, which requires the preparation of the data in similar ways—as is the case for data integration in general.

The chapter concludes with two case studies: one focusing on time series analysis to investigate global climate change; the other looks at the mapping of evapotranspiration in a lake ecosystem by using multiple sources of remotely-sensed data.

11.2 Observation models and process models

To study the relations between object properties and observed spectra, radiative transfer models have been developed. These models enable searching for optimum observation conditions and they can be used for the development of algorithms to retrieve physical properties of observed objects on Earth.

Radiative transfer models that describe the relations between physical and biochemical properties of objects on the one hand, and observed radiation on the other, can be called observation models. In an observation model, the characteristics of the observing instrument, the observational conditions and the observable object's properties all play prominent roles. Characteristics of the instrument and the observational conditions include the viewing direction, the spectral bands used and their spectral and spatial resolution. Object properties are, for instance, canopy LAI (leaf area index) for vegetation and suspended sediment concentration for water. Figure 11.1 illustrates the effect of vegetation canopy LAI on the observed reflectance spectrum in the visible, near infrared and shortwave infrared ranges. These simulations have been carried out with the well-known SAIL model. It demonstrates clearly that for the observation of high LAI values, especially the near infrared part of the spectrum is more sensitive to LAI than the visible part.

leaf area index

In the thermal infrared spectral region, surface temperature and emissivity are important object properties. Examples of other well-known physical theories in which the observation conditions play a central role are, for instance, Einstein's theory of relativity and the theory of quantum mechanics. Planck's law of black-body radiation can

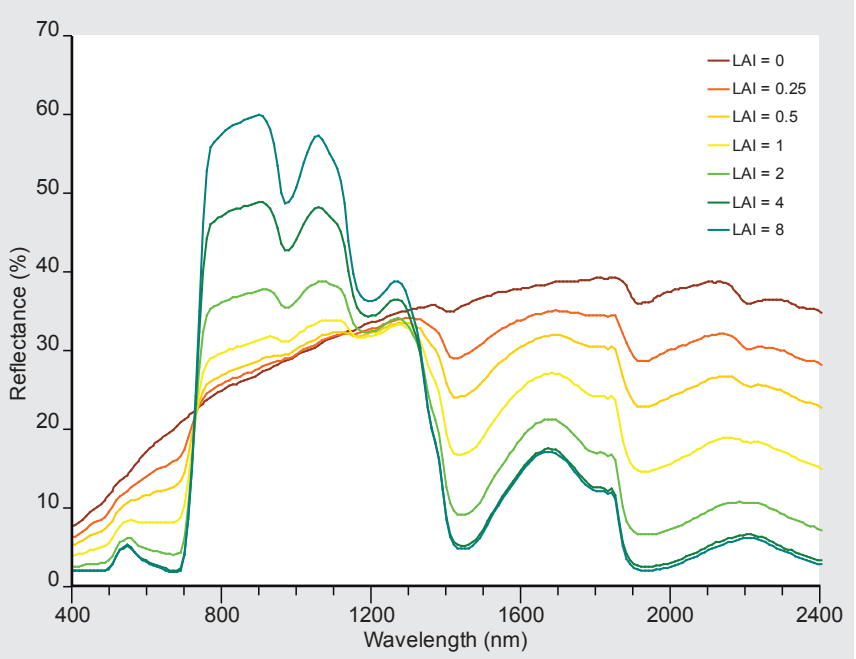

Figure 11.1
Changing vegetation spectra as a function of LAI.

also be considered an observation model as it predicts the observed radiation spectrum as a function of the object's temperature.

Most observation models relevant for remote sensing applications describe scattering and absorption of radiation in various media, such as the atmosphere, water bodies, snow, plant leaves and vegetation canopies. They might also include the scanning mechanism and other observational and instrumental properties, such as viewing direction, spectral and spatial resolutions, and signal-to-noise levels. Observation models may also be coupled. This is very useful, since most remote sensing observations involve a mix of several media, e.g. the combination soil–leaf–canopy and that of sea bottom–water–atmosphere.

On the other hand, we have process models in the Earth sciences that describe the evolution of geo(bio)physical surface properties in time, independently from remote sensing observations. Examples of such process models on various time scales are, for instance, numerical weather prediction models (NWPs), vegetation growth models, hydrological models, oceanographic models and climate models.

Process models in the geosciences usually rely on regular observations at many locations spread over a large area. Traditionally, these observations were mostly made in the field with a variety of instruments. Remote sensing techniques have tremendously increased the capability of spatial sampling and the consistency of the surface parameters measured. RS instruments are mostly sensitive to many physical properties of the surface, some of these may not belong to the set of properties that the user is interested in. Exceptions to this are the mapping of sea-surface temperature, laser altimetry and gravimetry, which are measurements of direct geophysical interest. In the majority of cases, however, there are only indirect relationships between what is observed with the instrument and the physical object properties of interest. In these cases, the use of observation models becomes an attractive option, since these models describe the relationships between all object properties relevant for the observation and the observed remote sensing data.

In general, remote sensing observations can be related to a number of object properties, but also to several other influences, for example atmospheric effects. On the other hand, some surface properties may have no effect at all on any of these observations. All these considerations lead to the following categories of physical quantities within the context of remote sensing:

Category 1 Primary RS observables, i.e. TOA (top-of-atmosphere) radiances;

Category 2 External variables that influence RS observables, e.g. atmospheric variables, Sun angle, view angle;

Category 3 Surface properties not of interest to users but which do have an influence on RS observables (e.g. leaf thickness influences leaf reflectance and transmittance, but will seldom be of interest to a user);

Category 4 Surface properties of interest to users that also have an influence on RS observables (e.g. leaf area index, LAI);

Category 5 Surface properties of interest to users that have no influence on RS observables (e.g. trace pollutants in water are of great interest but they are not detectable).

This is summarized visually in Figure 11.2. For users of remote sensing data, only quantities from category 4 are really of interest. Category 5 is also of interest to users, but undetectable by RS techniques. These quantities can only be measured by other means. Categories 2 and 3 have an impact on the observations, but are not of interest to users. Nevertheless, it is necessary to take them into account, since the observations are sensitive to these factors. Ignoring them might lead to an incorrect interpretation of the observed data.

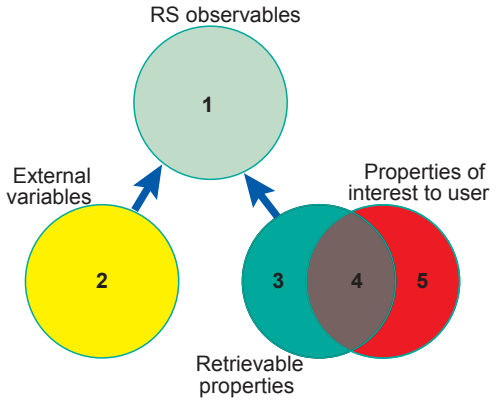

Figure 11.2
Earth Observation variables and their meaning for users. The numbers correspond to the five categories defined in text.

A complete observation model will describe the relations between quantities of categories 2, 3 and 4, on the one hand, and the quantities from category 1 on the other. Most radiative transfer models are, however, not complete, as they describe only radiative transfer in particular medium, such as water, soils, plant leaves, vegetation canopies or the atmosphere. Nevertheless, a complete observation model can be constructed by linking several sub-models together. This is not yet common practice, but is, nevertheless, strongly recommended since conclusions that are based on the interpretation of RS data with only one sub-model may not be reliable.

radiative transfer models

Finally, it should be noted that division over the five categories is not fixed but, rather, depends on the particular remote sensing techniques applied. For instance, object

height has no direct effect on passive RS observations, but it can be measured using active techniques such as laser altimetry. Besides, which properties are of interest to the user is strongly discipline and application dependent.

Observation models and process models can supplement each other to enhance the quality of the interpretation of remote sensing data and to fill gaps in time that occur when observations are not possible owing to clouds or some other cause. Figure 11.3 shows possible interactions of observation models and process models with EO data and existing geographic information (GIS and ground measurements, supplemented with decision-support systems (DSSs)). A central role is played by the GIS database, which provides a common geographic reference. The diagram shows how Earth observation data provide a series of snapshots of the situation on the Earth's surface (green triangle) and how this monitoring of the surface feeds a process model that is updated with actual data (purple triangle). The process model provides information to the decision-support system, which supports management actions aimed at controlling/mitigating the process. A good example of this is a water management system, in which one might decide to allocate water for irrigation if the observed vegetation appears to suffer from drought stress (see case study in Section 11.9).

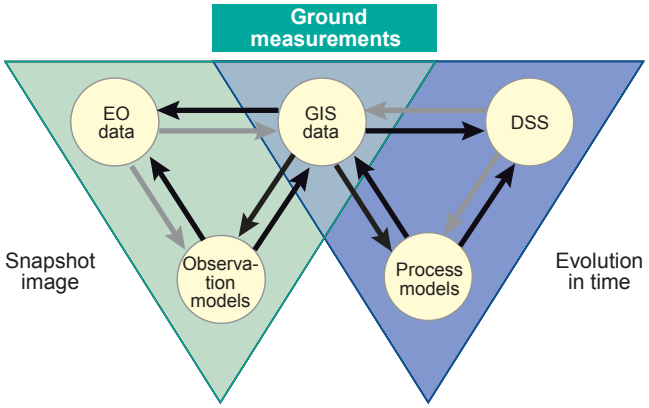

Figure 11.3
Interactions between observation models and process models. Light arrows indicate less likely (but possible) interactions, dark arrows the more obvious ones. The GIS database provides the common geographic reference.

GEOSS

The philosophy of combining many geospatial data sources in order to retrieve more and better information from Earth observation data is expressed in the GEOSS 10 year implementation plan [37], which states:

"Under GEOSS, national, regional, and international policy makers are collectively harmonizing observations, real- or near real-time monitoring, integration of information from *in situ*, airborne, and space-based observations through data assimilation and models."

How the concept of GEOSS could be applied in practice is illustrated in Figure 11.4, which shows a modelling system that simulates images recorded by various sensors on board Earth observation satellites. The heart of the system is a generic RS (observation) model that takes data from a GIS as input and produces as output simulated imagery at the correct spatial resolution and for the spectral bands of the simulated sensor. The RS model includes atmospheric effects and produces top-of-atmosphere (TOA) radiance images for all required spectral bands. The satellite data distributor also provides calibrated TOA radiance data, so this product can be compared to the simulated data.

This comparison is illustrated by the scale symbol, to illustrate the balance between the noise characteristics of the sensor, on one hand, and uncertainty in the surface properties on the other. If simulated and actual satellite images do not correspond

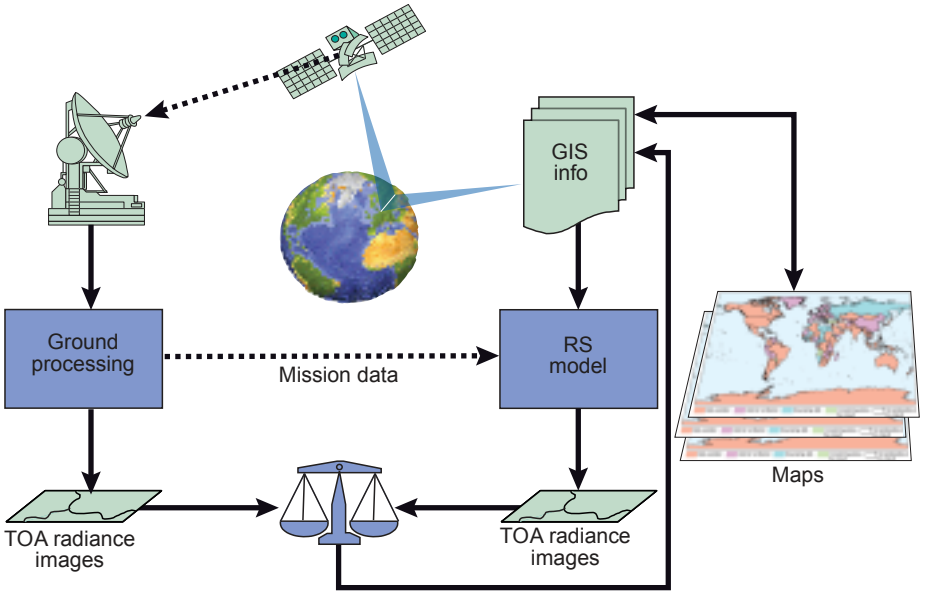

Figure 11.4
A generic image simulation system that produces images that can be compared to actual satellite images. A feedback mechanism minimizes the differences between both images by adjusting the GIS information. Updated GIS data may be transferred to new maps.

sufficiently well, the GIS information is adjusted until the error becomes acceptable. In the GIS, multiple layers of vector and raster data are stored and, in combination with attribute information and values of physical quantities expressing the surface properties, this information is used as input for the radiative transfer sub-models (e.g. for soils, leaves, vegetation canopies and the atmosphere) of the RS model. In other words, the GIS system provides the surface properties as well as their geographic location.

Both spatial data and attribute data (properties) can be in error, and different actions should be taken according to the kind of error. Geometric errors require a correction of the geographic position of one or more objects, whereas errors in surface properties only require the adjustment of these properties. Although the system as sketched is very complex, it has a high degree of flexibility with regard to sensors and geometries, so it would be possible to bridge gaps among the variety of sensor systems that are orbiting the Earth, thereby facilitating the assimilation of data from different sources (as promoted by GEOSS).

11.3 The *multi* concept in remote sensing

Remotely sensed data are often multispectral, sometimes multi-angular, and in some cases also multi-temporal, for instance when time series of satellite data are analysed to discover changes in surface properties or to monitor processes on Earth. If the spectral, angular and temporal domains are exploited to retrieve information about the surface, the data analysis and processing operations become more complicated, but one can retrieve more information from the data. This is why data integration is useful.

A few examples of multiple data observations are:

- colour photography
- multispectral remote sensing

- hyperspectral imaging
- multi-temporal image analysis
- multi-frequency and dual polarization SAR (synthetic aperture radar)
- multi-angular optical observations
- day–night thermal images.

An example of simulated multi-angular observations with a hyperspectral sensor is given in Figure 11.5, which shows how for a sparse vegetation object the observed reflectance spectrum in 201 bands changes with the image acquisitions from space under 7 different directions.

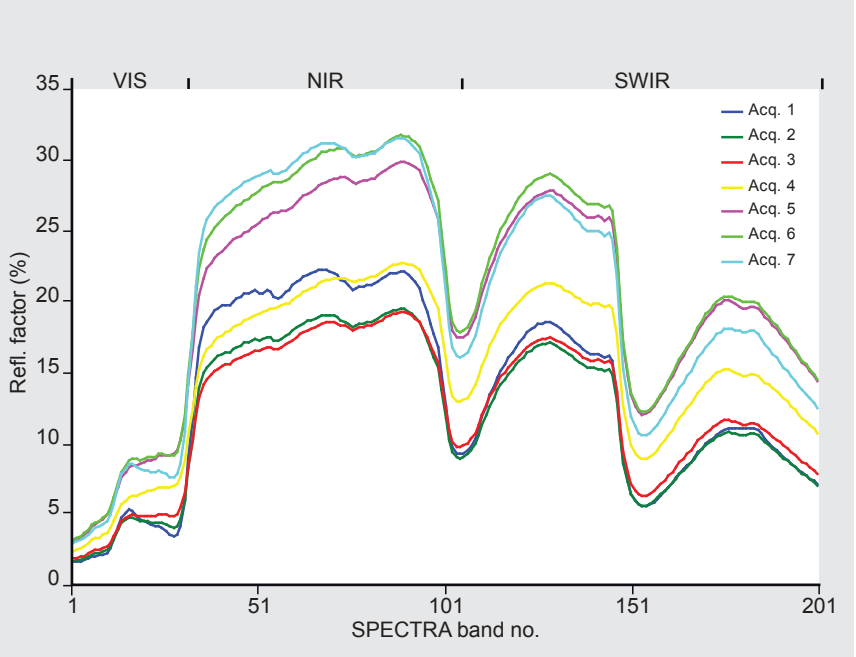

Figure 11.5
Surface spectra under different directions (model simulation)

Remote sensing data can not only be combined with other remote sensing data, but also with existing geospatial information, for instance the geographic information stored in a GIS.

Some examples are:

- digital elevation models (DEMs)
- land use information (GIS data)
- field measurements
- predictions from process models.

data assimilation

If predictions from process models are combined with remotely sensed data, the process model can be continuously updated with new observations. This is called data assimilation, a technique that is intensively applied in operational weather forecasting.

Combination of Earth observation data with other types of geospatial data is highly recommended since existing information can be essential for improving the interpretation of remote sensing data. The automatic classification of agricultural crops from multispectral image data is such an example. Pixel-by-pixel classification usually gives many errors, owing to sensor noise and field heterogeneity. However, if parcel boundaries are known from a GIS database, one can classify all pixels within a field as a group, which reduces the number of misclassifications enormously, provided, of course, that the group as a whole is correctly classified.

Data can be integrated in an almost infinite number of ways. Results from data integration can, again, be combined with other geospatial data to produce yet other new information, and so on. Therefore, only the most obvious forms of data integration will be dealt with in this chapter.

Although data integration can be very useful, there are also some requirements that have to be fulfilled for it to be effective:

- geospatial data have to be accurately co-registered in a common grid;
- time gaps between the various data layers have to be known and accounted for;
- systematic effects due to the atmosphere, the viewing angle, the Sun angle, etc., must be corrected for or taken into account.

In particular, if data from multiple sensor systems are integrated, one has to be aware of differences in their spectral sensitivities, wavelength bands, viewing angles, spatial resolutions, etc. Radiative transfer modelling can be applied to bridge the differences in spectral characteristics and viewing geometry of the various sensors. Other forms of modelling (e.g. 3D object modelling) are sometimes required to aid in the analysis of multi-angular data, for instance to differentiate true changes from apparent changes (e.g. shadows) due to a different viewing direction.

Data integration also comprises the incorporation of non-spatial information or *point* data from field measurements. These data have to be associated with precise moments in time and with precise geographic locations, or with some time interval and fuzzy-defined regions. Thus, here the important issue of the *representativeness* of this information for the associated time interval and geographic area comes into play.

representativeness

In general, data integration forces us to consider the uncertainties or inaccuracies of the various data sources available. In some cases, meta-data may contain information about this. When integrating data for some purpose, one has to apply weights to each of them, so that the final result is a balanced compromise in which inaccurate data receive less weight than those with a high degree of certainty.

The *multi* concept is often applied in remote sensing because multiple observations provide more information, in the sense that objects which look similar in a certain set of observables (spectral bands, times, angles) may look different if the number of observables is increased. A very simple example is the difference between a black & white and a colour photograph. Objects which look similar in black & white photograph may have totally different colours, so they become better distinguishable in a colour photograph. Another example, based on using multi-temporal data, can be found in objects that show similar behaviour as a function of time up until summer, but then start behaving differently. The difference will only become obvious if observations from both "before" and "after" are available.

the multi concept

In principle, multiple observations are always useful, since even if an observation is repeated under exactly the same circumstances with the same sensor (and thus might

rRetrievability

seem to be redundant) it is still of use as this helps to reduce the influence of noise. Statistically, the uncertainty of a mean value is inversely proportional to the square root of the number of repeated observations. If the observations are made with multiple sensors, then they provide more information, because different characteristics are measured. For the retrieval of surface properties from Earth observation data it is important to consider which factors determine the retrievability. Of course, only surface properties to which the observations are sensitive can in principle be retrieved, but it is equally important that a change in another surface property does not produce a similar response in the observations. This is the issue of linear dependence. If two surface properties produce a proportionally equal response in all observables (i.e. spectral bands, moments of observation, viewing directions), then there is linear dependence, and one cannot determine which surface property was the cause of the observations. In Figure 11.6, three different situations are illustrated for the case of two surface properties and two observables.

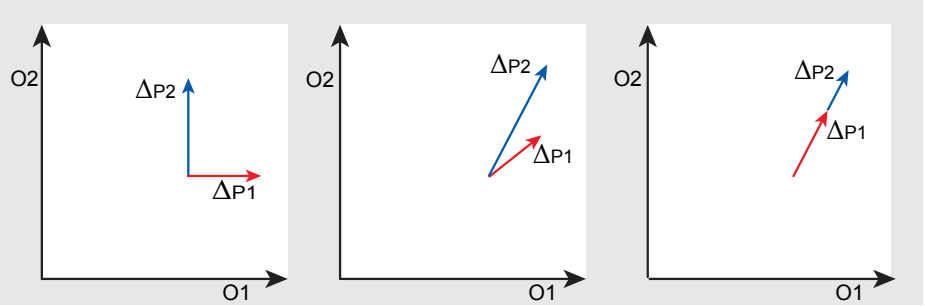

Figure 11.6
Linear dependance: two observables (O) and two surface properties (P).

In the left-hand diagram, property 1 only influences observable 1, and property 2 influences only observable 2. This case is very extreme and seldom occurs in practice, but the conclusion we can draw from the diagram is that in this case property 1 should be estimated from observable 1 and property 2 from observable 2. The middle diagram shows the more common situation that both surface properties influence both observables, albeit in different ways. In this case both properties can still be retrieved mathematically, since we can solve the associated system of two equations with two unknowns. The right-hand diagram illustrates the case of linear dependence. A change in both properties produces a similar change in the observables—perhaps of a different magnitude, but in the same direction. In this case one cannot retrieve both properties separately.

To summarize, the two main conditions for good retrievability are a high sensitivity and linear independence. The chance of encountering cases of linear dependence decreases with the number of independent observations, and since multiple observations are mostly independent, more surface properties can be retrieved and with a higher accuracy.

An inherent part of the analysis, as well as the representation, of multiple observations is visualization. Many visualization techniques have already been explained in Chapter 10, but some additional techniques are shown in Sections 11.7–11.9 to show how linear changes and the dynamics of periodic processes can be visualized.

11.4 Spatial, temporal and spectral scales

In the spatial, temporal and spectral domains that play a role in Earth observation, one can define the concepts of resolution, sampling interval and scale. Resolution describes the ability to resolve small details (in space, time or the electromagnetic spectrum). Sampling interval refers to the distance between two successive observations, while scale describes the total range of observations in a collection of data.

According to the sampling theorem of Nyquist and Shannon, which states that

> "If a function $x(t)$ contains no frequencies higher than B hertz, it is completely determined by giving its ordinates at a series of points spaced $1/(2B)$ seconds apart",

the ideal sampling interval should be equal to half the resolution, which means two samples per resolution cell. Otherwise, one loses information (under sampling) or one samples more densely than necessary (oversampling). In practice, however, sampling interval and resolution are often roughly equal, although it is good to keep in mind that resolution and sampling interval are two different things. Note, by the way, that in the above example the time domain was taken as the basis, but in the spatial domain the same considerations apply.

resolution vs. sampling interval

Scales are more applicable to processes in the spatial and temporal domains than to those in the spectral domain. For a number of important Earth system processes, their corresponding scales are roughly indicated in Figure 11.7, which has logarithmic X- and Y-axes in order to accommodate the large ranges to be considered in the spatial and temporal domains. In the spatial domain this goes from 1 mm to 40,000 km (the circumference of the Earth), and in the temporal domain from one second to a century.

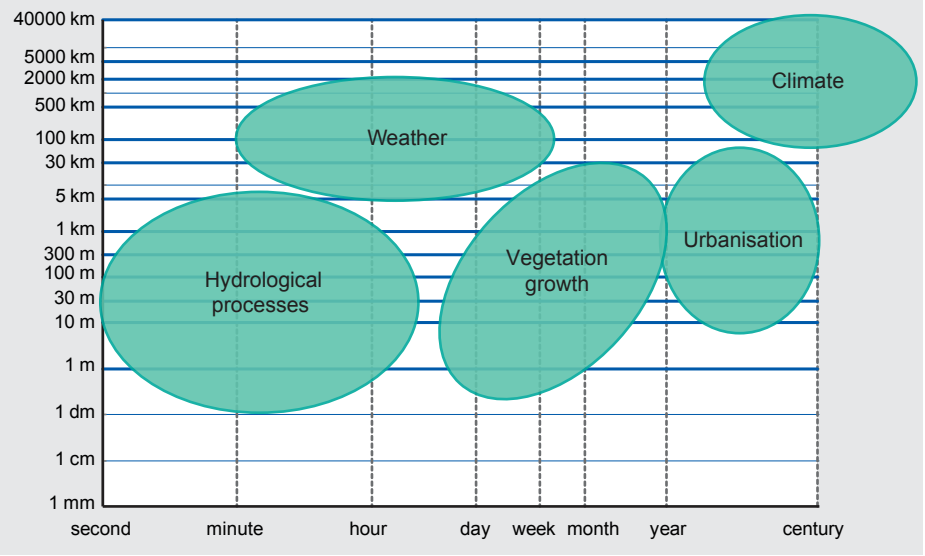

Figure 11.7
Temporal and spatial scales of some Earth system processes.

Spatial and temporal scales can not only be attached to processes, but also to observations. An example is given in Table 11.1, which summarizes the spatial and temporal scales of a few well-known Earth observation systems.

As well as spatial, temporal and spectral scales, which are more related to the act of making observations, it is equally important to consider different levels of spatial

Table 11.1
Scales of RS observations.

Sensor	Spatial scale	Temporal scale
Meteosat	Hemisphere	15 minutes
NOAA-AVHRR	3000 km	daily
Landsat TM	180 km	16 days
SPOT	60 km	26 days (pointable)

levels of spatial aggregation

aggregation in various Earth science processes. These aggregation levels are mostly ordered hierarchically. For instance, a forest consists of trees, which have trunks, branches and twigs, on which one finds leaves or needles, and so on. Similarly, an agricultural area may be described in terms of parcels, lots, cropping fields, individual plants, stems and single leaves.

Analysing multiple layers of geospatial data in a meaningful and coherent way requires the co-registration of all these layers to a common spatial grid or reference. The common grid spacing chosen is application-dependent and several considerations may play a role in that choice. In some cases the preservation of high levels of spatial detail is most important, and in other cases high levels of radiometric precision may be more relevant. In the first instance, one would probably choose a common grid spacing that accommodates the data layer with the highest spatial resolution, while in the second instance one may choose a grid with a wider spacing. Figure 11.8 illustrates the display of two images with different grid spacing and orientation for a part of Enschede. The images have the same georeference, yet the pixel size and orientation are different

resampling and aggregation

A common grid also requires a *resampling* of those layers that have a different spacing and/or orientation. In some cases, especially when an image of high spatial resolution is converted to a less dense grid, the resampling has to be combined with *aggregation*, e.g. implemented as a low-pass filter applied to the input layer so as to exploit the high spatial density of that layer, in order to increase the radiometric accuracy and thus reduce noise.

In addition to spatial resampling and aggregation, other operations sometimes have to be applied to the data to condition them for data integration. This would be necessary when, for example, analysing a long time series of satellite data for which the calibration data have gradually changed in the course of time—or even suddenly, for example owing to the replacement of an existing satellite with a new one. In such cases, the calibration data have to be corrected in order to obtain a time series that is free of these artefacts.

Sun-synchronous

In time-series analyses of NOAA AVHRR data, however, another gradual effect was observed that could not be corrected. This effect is known as the orbital drift problem. Each NOAA satellite has a Sun-synchronous orbit that is not very precise, which means that after a number of years the moment in time at which the Equator is crossed gradually increases by a couple of hours. See Figure 11.9, which illustrates this for several satellites from the NOAA series. This means that observations coming from a satellite that is at the end of its life are not comparable to similar observations made at the beginning of its life. Especially in the Southern Hemisphere, this led to local solar times of observation very late in the afternoon. However, effects caused by drastically changing illumination conditions cannot be corrected, so in such cases one has to reject data if conditions deviate too much from normal.

If the calibration data of one or more satellites have changed, we can sometimes compensate for these effects by using a target on Earth that has stable reflectance proper-

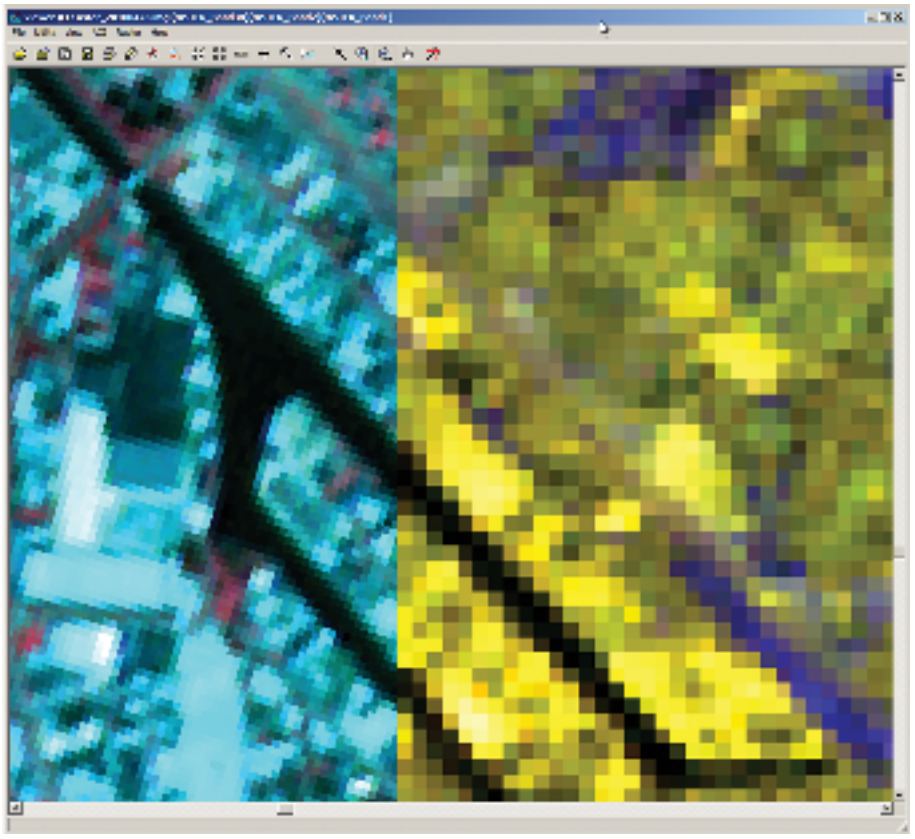

Figure 11.8
Difference in grid spacing and orientation.

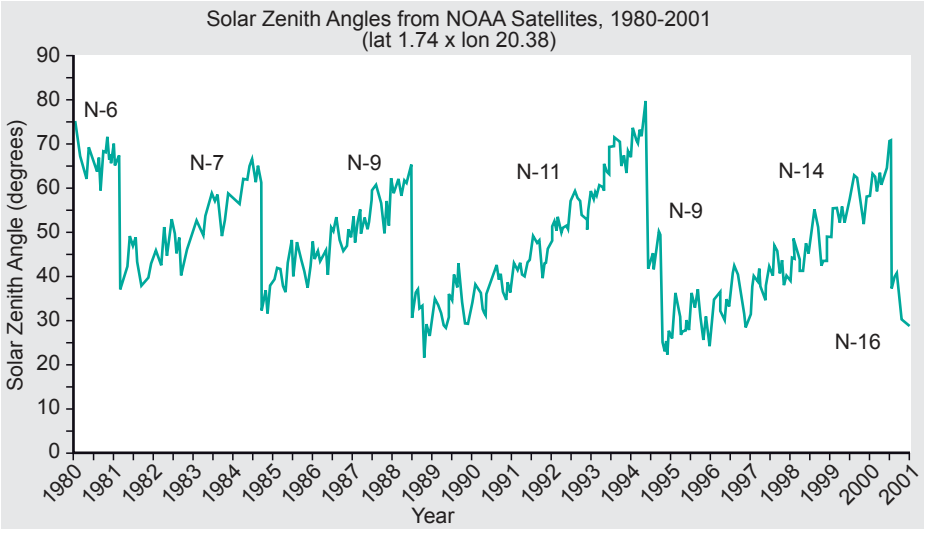

Figure 11.9
Course of the local solar time of observation near the Equator from 1980 to 2001 for the NOAA series of satellites. Source `http://classic.nerc.ac.uk/`

ties. In one such case, the Libyan desert in Africa was used as a stable reference target with a constant NDVI value, and all data were recalibrated so that the same NDVI resulted for that area during the whole time series of 18 years.

If two sensors with different spectral characteristics are involved in the data integra-

tion, then one can try to match the spectral bands of one sensor with the closest bands of the other sensor, but one has to be careful in doing so, since subtle spectral differences between objects on the ground will be observed differently by both sensors, so this cannot be completely corrected. Figure 11.10 shows the spectral response functions for the ASTER and MODIS sensors on board the Terra satellite, together with some spectra of surface reflectance. This clearly illustrates the problem of combining different sensors in spectral regions where surface reflectance is rather variable, such as in the so-called red-edge region (around 700 nm).

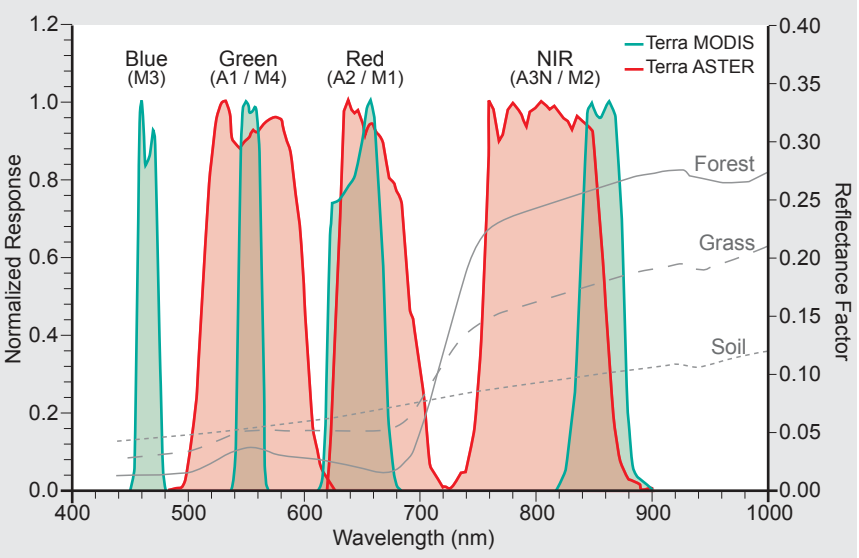

Figure 11.10
Spectral response functions for the ASTER and MODIS sensors on board of the Terra satellite and reflectance of three surface types. Source: [75].

Similar considerations apply in the case of multiple observations from different satellites that are treated as synoptic observations of one moment, while actually there may be a time difference of days or a local time difference of hours. These cases are very difficult to handle correctly, but radiative transfer modelling can be applied to bridge the difference in the Sun–target–sensor geometry and process models might be used to account for time differences.

Apart from the more sensor-based data-conversion issues already mentioned, sometimes conversion operations are also necessary to bridge differences in data formats related, for example, to:

- computer data types (byte, integer, float)
- image data organization types (raster BIL, BSQ and BIP formats)
- image data formats (JPEG, GIF, BMP, GeoTIFF, HDF, etc.)
- raster <> vector (points, lines, polygons)
- vector TIN to contour lines
- physical unit conversion.

11.5 Data integration issues in GISs

Integrating data sets in a GIS often results in an improved understanding of the problem/phenomenon at hand. One could even say that data integration is the raison d'être of GISs; in any case, data integration certainly facilitates further analysis of the data.

In real-life projects the user often has to integrate data by:

- merging mismatched data layers
- choosing, in cases where two data sets of the same features exist, which set should be preferred (based on criteria that need to be defined);
- solving, for example, problems such as changes in administrative units (merging or splitting of areas) and matching these with data that only refer to an administrative name or code.

Moreover, there is always a need to merge non-spatial (statistical data, social behaviour data, ...) with spatial data. With volunteered geodata and with crowdsourcing (Web 2.0), data integration becomes both more tricky and also more important. In this respect, meta-data and lineage documentation are essential for proper data integration. The merging of mismatching data layers might require dealing with:

- mismatchings in area (spatial extent)
- mismatchings in level of detail (scale)
- mismatchings in projection (georeferencing)
- mismatchings in time
- mismatchings in accuracy
- mismatchings in data format/type (tabular and spatial data)
- mismatchings in purpose for which the data are being collected.

11.6 Change detection

Change detection is a particular application of Earth observation in which data integration is required before one can concentrate on the observable changes. This application is susceptible to the problem that changes in the observation system can be confused with the actual changes in the target objects themselves. Once again, in this case radiative transfer and observation modelling, adapted to the sensors at hand, may help to separate apparent changes from true changes. Here, true changes are changes in the object properties, while apparent changes are only related to changes in the observation conditions.

true and apparent changes

In change detection, there are different kinds of change to be distinguished:

- *Gradual changes* (sometimes called linear changes) are involved in climate change investigations, deforestation, urbanization, etc.
- *Sudden changes* are mostly related to disasters (floods, earthquakes, volcanic eruptions, fires, etc.)

- *Periodic changes* are related to the daily and yearly cycles of solar illumination and warming, giving rise to the diurnal cycles of daylight and temperature and the seasonal patterns of vegetation growth.

This section will focus on how data integration is applied in change detection. We will focus on changes on the surface of the Earth, but there is certainly an overlap with the techniques used in other image processing sciences, like medical imaging.

Changes are caused by processes. These processes can be natural, man-made, seasonal, deterministic or random. To determine appropriate data sources for detecting change, several characteristics of the process need to be known, such as speed, duration, observables, area coverage and seasonality. Section 4.7.1 (and Section 11.1 and Figure 11.2) explains how these characteristics can be used to determine spatial and temporal coverage, time and frequency of observation, spatial resolution or scale, and observables. The expected size of the change determines the degree of sensitivity needed in the analysis.

Change detection can be carried out at various levels of detail or sophistication, depending on the interests of the user. This may include answering some or all of the following questions:

- Has there been a change (detection)?
- What is the nature or type of the change (identification)?
- What is the area covered by the change (area)?
- What is the spatio-temporal pattern of the change?

Over the years, several categories of change detection techniques have been developed. These techniques will be discussed in the remainder of this subsection, focusing on whether they can be used for detection, identification, area and/or spatio-temporal patterns of change. The definition and description of categories is mainly based on [70].

Algebra techniques for change detection

This group of techniques includes all kinds of algorithms that are based on combinations of values of a pixel in subsequent images, such as image differencing, image ratioing, vegetation index differencing, image regression and change vector analysis.

image differencing

Image differencing is a band-by-band, pixel-by-pixel subtraction of two images whereby the resulting change image has the same number of bands as the input images. Each band of the change image contains the differences between the spectral values of the pixels in the two original bands.

image ratioing

Image ratioing is a band-by-band, pixel-by-pixel ratio of two images whereby the resulting change image has the same number of bands as the input images. Each band of the change image contains the ratios of the spectral values of the pixels in the two original bands.

vegetation index differencing

For vegetation index differencing, vegetation index is calculated for each image; the change image contains the differences between the vegetation indices for each pixel.

image regression

For image regression, a relation is established through regression between two images of different dates. The relation is used to predict pixel values in the second image, which are then subtracted from the first image. Regression reduces the effects of sensor, atmospheric and environmental differences between the two images. Development of suitable regression functions can be difficult.

change vector analysis

In change vector analysis a spectral change vector is calculated, which describes the direction and magnitude of the change between two dates and a total change magnitude for each pixel. The total change equals the Euclidean distance between end points in an n-dimensional change space; any number of spectral bands can be processed in this way. The method produces detailed change information.

All methods in the "algebra" category rely on the selection of a threshold on the change image, to separate noise and apparent changes from true changes and to determine the change areas. The choice of the threshold is often difficult and arbitrary. With exception of change vector analysis, these methods cannot provide a complete change matrix, so there is no complete identification of the nature of all changes. Algebra is often used when the focus is on detecting a very specific change, for example detection of forest fires, where changes in the thermal bands indicate a rise in temperature of the land surface and a threshold determines whether or not there is a fire. Other common applications include deforestation mapping and detection of vegetation change.

change matrix

Classification-based change detection

The techniques in this category all involve some kind of classification of separate or combined images. Some of the most common techniques are discussed in the remainder of this subsection. For a more exhaustive list, see [70].

post-classification comparison

In post-classification comparison, the images are classified separately and classifications at different dates are compared. The advantages of this technique are the minimization of atmospheric influences and the fact that it generates a complete change matrix. The disadvantages are that sufficient training data are needed for each classification (date) and that there might be systematic differences between both classifications.

spectral-temporal analysis

For spectral-temporal combined analysis, all images are stacked in one data set and classified together, all at once, similar to a multispectral classification with many bands. Changes are identified and labelled. This can be time-saving, but it may be difficult to identify and label the change classes. A complete change matrix cannot be provided.

unsupervised change detection

Unsupervised change detection labels spectrally-similar groups and clusters at Date 1, followed by spectrally similar groups at Date 2, and then detects changes. Because an unsupervised algorithm is used, the process can be automated, but labelling the changed areas is not always straightforward, especially in the case of processes (i.e. a series of changes that are part of a process, such as conversion of forest via burnt areas to crops and, finally, pasture).

hybrid change detection

Hybrid change detection first isolates changed pixels to construct a binary change mask. The change mask then sieves out the changed themes from land use/land cover (LULC) maps.

Visual analysis for change detection

The human eye is still one of the most powerful instruments available for detecting and interpreting change. Visual interpretation can be aided by different ways of displaying time series, such as multi-temporal colour composites and animations. Results depend very much on the skills of the analyst and their familiarity with the area.

GIS

GIS overlays

Change can also be detected by combining maps and images. GIS overlays on image data can provide a means for better interpretation and for detection of changes, e.g. new buildings, changes in parcel boundaries or forest limits. The results can be directly combined with other data in the GIS, for example to update LULC information. The difficulties lie in reconciling the accuracy of different sources and their registra-

tion.

Past and current maps of land use/land cover can also be combined and, if necessary, integrated with topographic and geological data. In addition to difficulties arising from differences in accuracy of the sources and their registration, thematic categories in the maps may not always match.

Other methods

transformations

Transformations are essentially data reduction techniques, which reduce redundancy between bands or images and highlight any differences. They have been applied to change detection, but the disadvantage of such transformations is that they cannot produce detailed change matrices, they require (arbitrary) thresholds, and it is difficult to interpret and label the change information they generate.

model-based methods

A number of model-based methods have been developed for very specific purposes. These include the modelling of reflectance of certain classes or for the retrieval of biophysical parameters from spectral characteristics.

object-based change detection

Furthermore, new developments in image classification also result in new approaches to change detection. Image classification based on objects (object-oriented analysis) is employed in change detection. Fuzzy classification allows for the fact that boundaries can be vague or gradual and developments in this field also lead to the development of change detection methods that can adequately deal with changes in gradual boundaries or in objects with vague boundaries. This approach is, however, beyond the scope of the Core module.

The case study on climate change described in Section 11.7 is an example of how one can analyse a mixture of periodic phenomena (annual vegetation growth) and gradual changes (year-to-year variations).

11.7 Case study: Climate change

To find evidence for the impact of climate change on processes on Earth, time series of satellite images are particularly suitable, since they constitute regular observations over a long period of time under comparable conditions. Many processes on Earth are controlled by the yearly seasonal cycle and can, therefore, be roughly modelled as periodic functions, although these processes are also gradually evolving owing to climate change. In order to find evidence for climate change, long-term trends have to be separated from seasonal effects. This can be done by estimating the periodic parameters of each year and by analysing trends in those annual parameters. In this case study, a time series of NOAA NDVI images of the world was analysed to discover trends in global vegetation-growth patterns over the period 1982–2000. In most years, 36 images of the 10-daily maximum NDVI were used as input.

maximum value compositing

The maximum value compositing (MVC) technique is often applied to time series of NDVI images in order to reduce the effects of cloud cover, atmospheric conditions and large viewing angles. During a 10-day period the NOAA satellite views a given location on Earth every day at approximately the same local solar time, but the viewing angle and the atmospheric conditions may vary a lot during this period. As the NDVI is always *decreased* under cloudy or hazy conditions, as well as for large viewing angles, by taking the maximum NDVI of the 10-day period one hopes that the best observation has been selected. This method removes most cases of cloud cover in most regions, but when the NDVI of a certain location is plotted as a function of time, one still sees some residual effects of cloud and haze.

The HANTS (harmonic analysis of time series) algorithm works similarly to MVC by removing negative outliers, not within 10-day intervals but over the whole year. In this case, the signal is modelled by a series of sine and cosine functions that span the whole period and have frequencies corresponding to the base period (e.g. one year) and a number of higher harmonics (waves of higher frequency that fit in the base period). As illustrated in Figure 11.11, negative outliers are removed and a gentle curve is fitted to the remaining points.

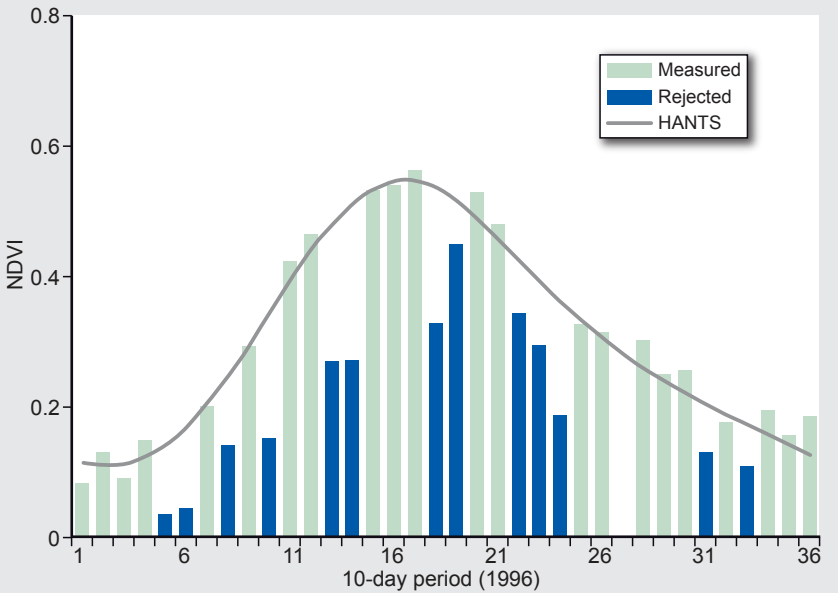

Figure 11.11
Outlier removal and curve fitting using the HANTS algorithm.

Provided a phase is assigned to each frequency, the series of sine and cosine functions can also be expressed as a series of only cosine functions:

$$y(t) = a_0 + \sum_{i=1}^{n} a_i \cos(\omega_i t - \varphi_i), \tag{11.1}$$

where $a_0 \ldots a_n$ are the amplitudes and $\varphi_1 \ldots \varphi_n$ the phases. The circular frequencies $\omega_1, \ldots, \omega_n$ are chosen in such a way that $\omega_i = \frac{2\pi}{T} i$, where T is the length of the base period. The amplitude of the zero frequency, a_0, plays a special role, since it equals the mean value of the modelled time series. To model vegetation dynamics throughout the year, three frequencies above the zero frequency are usually sufficient. This also means a considerable data reduction, since 36 original data points are then represented by only seven components, namely the mean and, for the three frequencies, the amplitude and the phase.

Modelling with a higher number of frequencies allows more details of the original series to be preserved, but then there is a chance that effects due to cloud and haze are preserved as well. Vegetation growth, on the other hand, is usually a fairly gradual phenomenon and three frequencies are sufficient to follow the most rapid growth spurts. Figure 11.12 visualizes the results for one year (1995) of data for the world.

This kind of visualization reveals that the frequencies 2 and 3 (periods of 6 and 4 months, respectively) are already quite noisy owing to residual cloud cover and haze effects. The mean, the yearly amplitude and the yearly phase look most reliable.

The phase is a number ranging from 0 to 360° or, if expressed in radians, from 0 to 2π. Showing the phase as an image in black & white creates a problem, since 0° would be shown as black and 360° as white, while actually 0° and 360° represent the same angle. In this case one can use a colour look-up table that is circular in the RGB values, meaning that 0° and 360° are represented by the same colour. A *rainbow* look-up table (LUT) can be constructed in such a way that it follows the colour sequence blue-cyan-green-yellow-red-magenta-blue, so that the start and the end have the same colour. Such a LUT was applied to the phase images of Figure 11.12.

Phase information is independent of amplitude, but in practice one would like phase information to be considered less important for small amplitudes. The following set of equations provide a way of accomplishing a colour transformation that is controlled not only by the phase but also by the amplitude:

$$R = 127 \times \left[1 + \frac{A}{A_{max}} \cos(P - 240)\right]$$

$$G = 127 \times \left[1 + \frac{A}{A_{max}} \cos(P - 120)\right]$$

$$B = 127 \times \left[1 + \frac{A}{A_{max}} \cos(P)\right]$$

Here P is the phase in degrees, A the amplitude, and R, G and B are the amounts of red, green and blue on a scale from 0 to 255. The constant A_{max} is the maximum expected amplitude. If the amplitude equals the maximum amplitude, the RGB values vary from zero to 254, so a large colour saturation is obtained. This is also demonstrated by Figure 11.13, which shows the curves for R, G and B as a function of P if $A = A_{max}$.

For zero amplitude R, G and B all become equal to 127, so one will observe mid-grey.

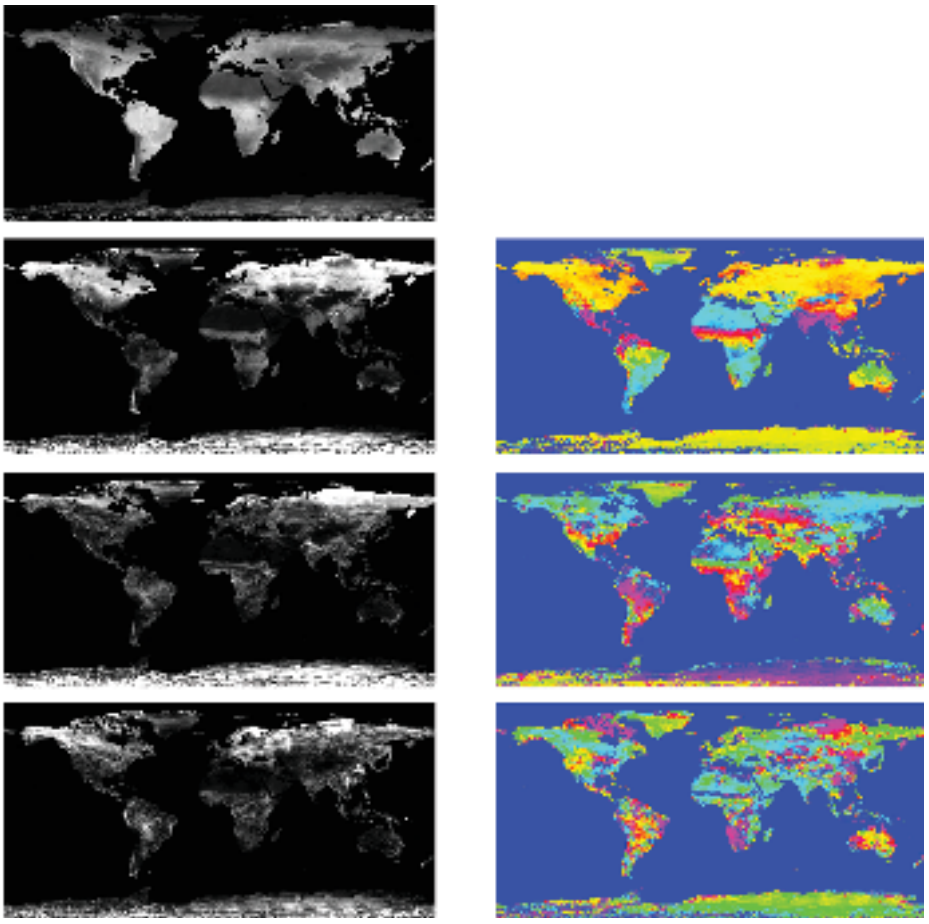

Figure 11.12
Global NDVI dynamics for the year 1995. Amplitudes are in the left-hand column; phases are in shown in the right-hand column in rainbow colours. Frequencies (top to bottom) = 0, 1, 2, 3.

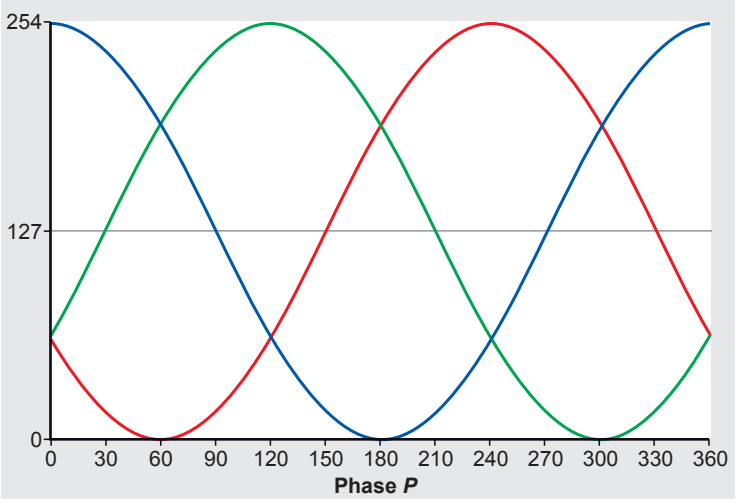

Figure 11.13
Variation of R, G and B as a function of the phase angle P.

It is also possible to include mean NDVI by coupling it to the pixel's intensity. In this case the factor 127 in the above formulas is replaced by

$$\frac{M - M_{\min}}{M_{\max} - M_{\min}} \times 255,$$

where M is the annual mean NDVI. This method of visualization was applied to global data: Figure 11.14 shows global NDVI dynamics for all years from 1982 to 2000.

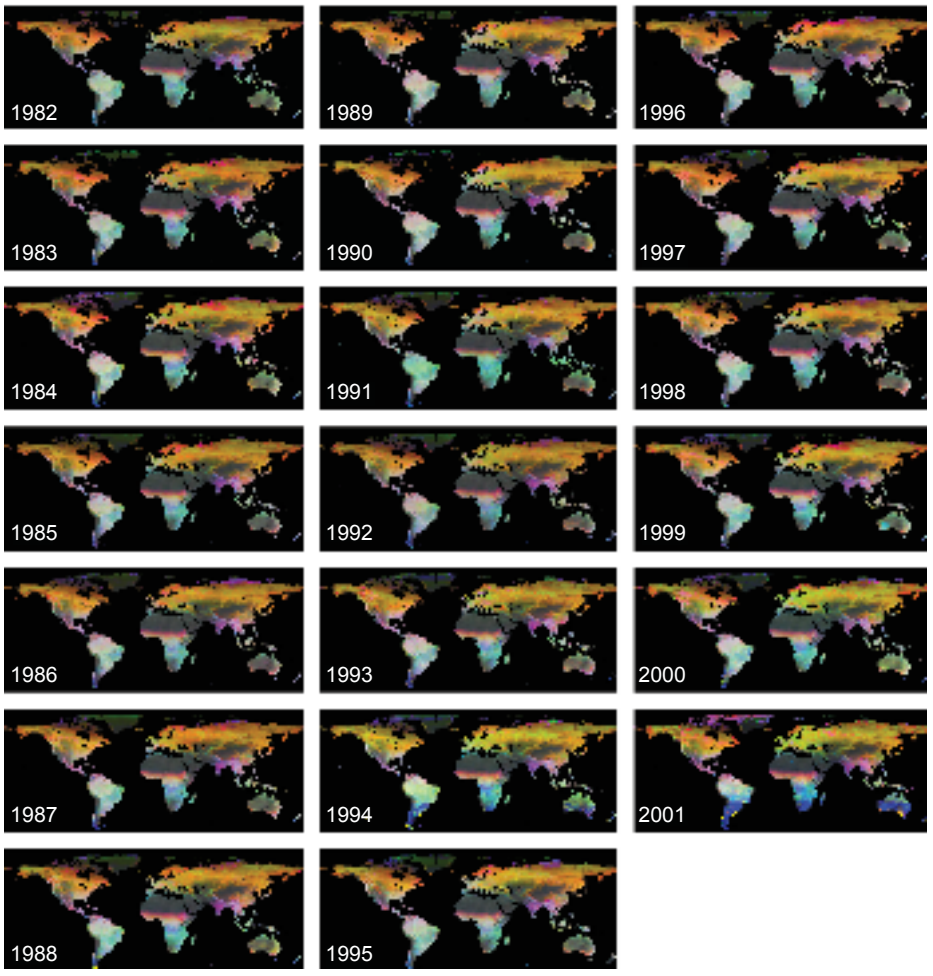

Figure 11.14
IHS representation of global yearly vegetation dynamics for the years 1982–2001. Note anomalous behaviour in southern areas in the years 1984, 1988, 1993+1994 and 2000+2001 owing to the problem of orbital drift.

In order to obtain evidence of climate change, trends in the changes of mean NDVI, its yearly amplitude and its phase were analysed by correlating these quantities with time. In addition, the start and the end of the growing season were established from the yearly growth patterns by finding the intersection of the growth curve with fixed NDVI levels. Next, simple linear regression analysis was applied for each pixel to find the rate of change (i.e. the slope of the regression line) at each location. To display the results, a colour look-up table was used in which negative slopes were shown in blue, positive slopes in red, and zero slopes in white; the degree of colour saturation was used to show the magnitude of the slope.

The result is shown in Figure 11.15, which indicates that trends in vegetation dynamics have taken place all over the world in this period of 20 years. These trends are characterized by a slight increase in annual mean NDVI, increasing as well as decreasing yearly amplitudes, an advancement of the yearly phase, an advanced start

of the growing season, and a lengthening of the growing season. These phenomena are due to increasing global temperatures, especially in winter; CO_2 fertilization; and advances in agrotechnology.

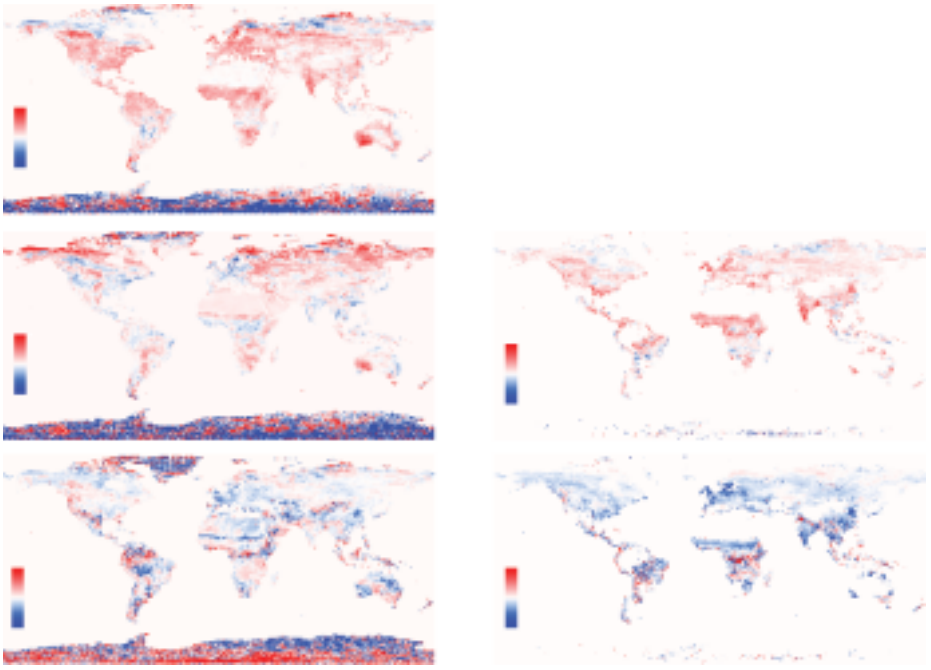

Figure 11.15
Global trends (increase per year) in (left-hand column) mean NDVI (range -0.01–0.01), yearly amplitude (range -0.01–0.01), yearly phase (range -5:5 deg); and (right-hand column) length of the growing season (range -10–10 days) and start of the growing season (range -5–5 days).

Note that in Antarctica strong trends are also found. However, these have to be considered as unreliable as the associated correlations were not significant. If we only take into account the locations where the correlation coefficient is significant at the 5% confidence level (for 20 observation this means a minimum absolute correlation of 0.45), then the picture shown in Figure 11.16 is obtained.

One can observe in Figure 11.16 that that significant trends are especially clear for India and the Sahel region in Africa and that the clearest trends are indicated by the increasing mean NDVI and the longer growing season in these regions.

These results are based on 20 years of NOAA-AVHRR data, which actually comprised 36 maximum-value composites of the 365 daily NDVI images per year. The NDVI is, in turn, based on the red and near-infrared spectral channels, and the original ground resolution of these GAC (global area coverage) data was 4 km at nadir. These data were aggregated by the satellite data distributor into $1^\circ \times 1^\circ$ geographic cells before their dissemination to users. Roughly estimated, $20 \times 365.25 = 7305$ satellite images in two channels have contributed to the final result (indicating climate change) for each single $1^\circ \times 1^\circ$ pixel, so this represents an extreme example of data integration.

The visualization technique presented in Figure 11.14 for the whole world has been applied to smaller regions as well, using SPOT-VGT NDVI images as input. Only data from the year 2002 were processed to show the influence of topography on vegetation-growth dynamics. In order to express the terrain topography in the image, a technique called hillshading was applied. Here, data from a digital elevation model (DEM) were integrated with the NDVI dynamics by modulating them with the resulting hillshading, as shown in Figure 11.17; the colour circle indicates which colour hue is to be associated with the month of maximum NDVI.

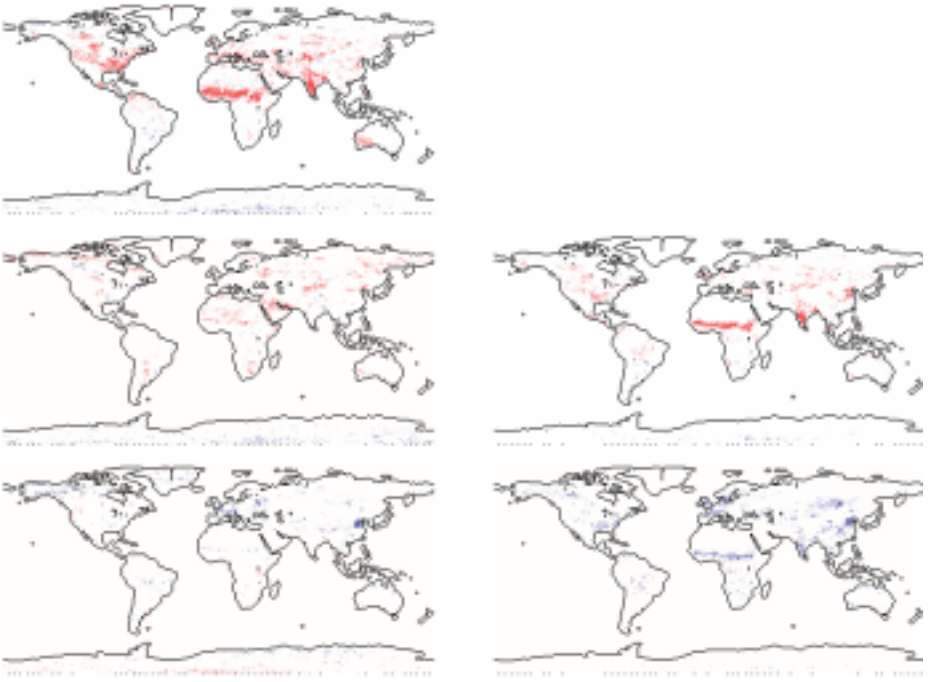

Figure 11.16
Significant (5% confidence level) correlation coefficients (absolute value > 0.45) for trends corresponding to those shown in Figure 11.15. Positive trends are shown in red, negative trends in blue.

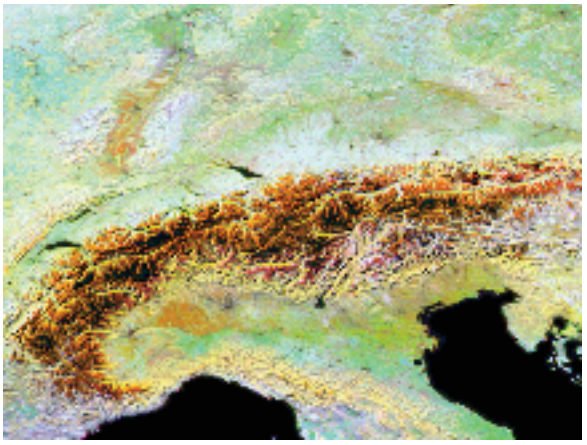

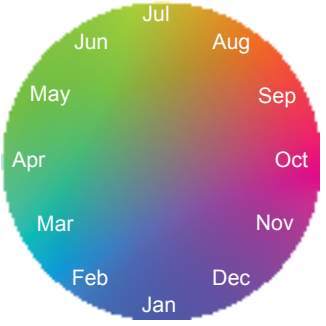

Month of maximum green vegetation (NDVI) and related colour

Figure 11.17
Vegetation dynamics in 2002 of the Alps and surroundings. The colour circle shows the relation between the month of maximum NDVI and the colour hue.

In this image, one can observe a strong relation between topography and vegetation growth. The Alps show red and brown colours, indicating maximum NDVI in August–September. This is because in mountainous regions there is snow in winter and spring, which delays growth. In very high regions, snow cover is permanent. These have no vegetation at all during the whole year, so they appear black. In the image one can also clearly recognize the Upper Rhine Valley (orange), the Black Forest (white), the Po Valley and the Apennines in Italy, and a large area west of Milan where rice is grown (orange). The grasslands to the north of The Alps are white, indicating permanent green vegetation cover throughout the year.

The same SPOT-VGT data for the whole of Europe were used to make a cloud-free, synthesized time series of images that show winter snowfall and its withdrawal in spring and summer. In this case the original SPOT bands in the red, near infrared and

shortwave infrared were used, and positive outliers were removed using the HANTS algorithm to obtain cloud-free data. Snow has a high reflectance in the visible and the near infrared, but it absorbs radiation in the shortwave infrared. In an RGB composite of NIR, SWIR and RED (in that order), snow appears in purple (magenta), since the SWIR component is missing, and only NIR and RED remain, which control red and blue, respectively, so we obtain magenta colours. Such a sequence of images can be played as an animation, which is an alternative way of observing the processes of vegetation growth and snow cover. The individual images are shown in Figure 11.18.

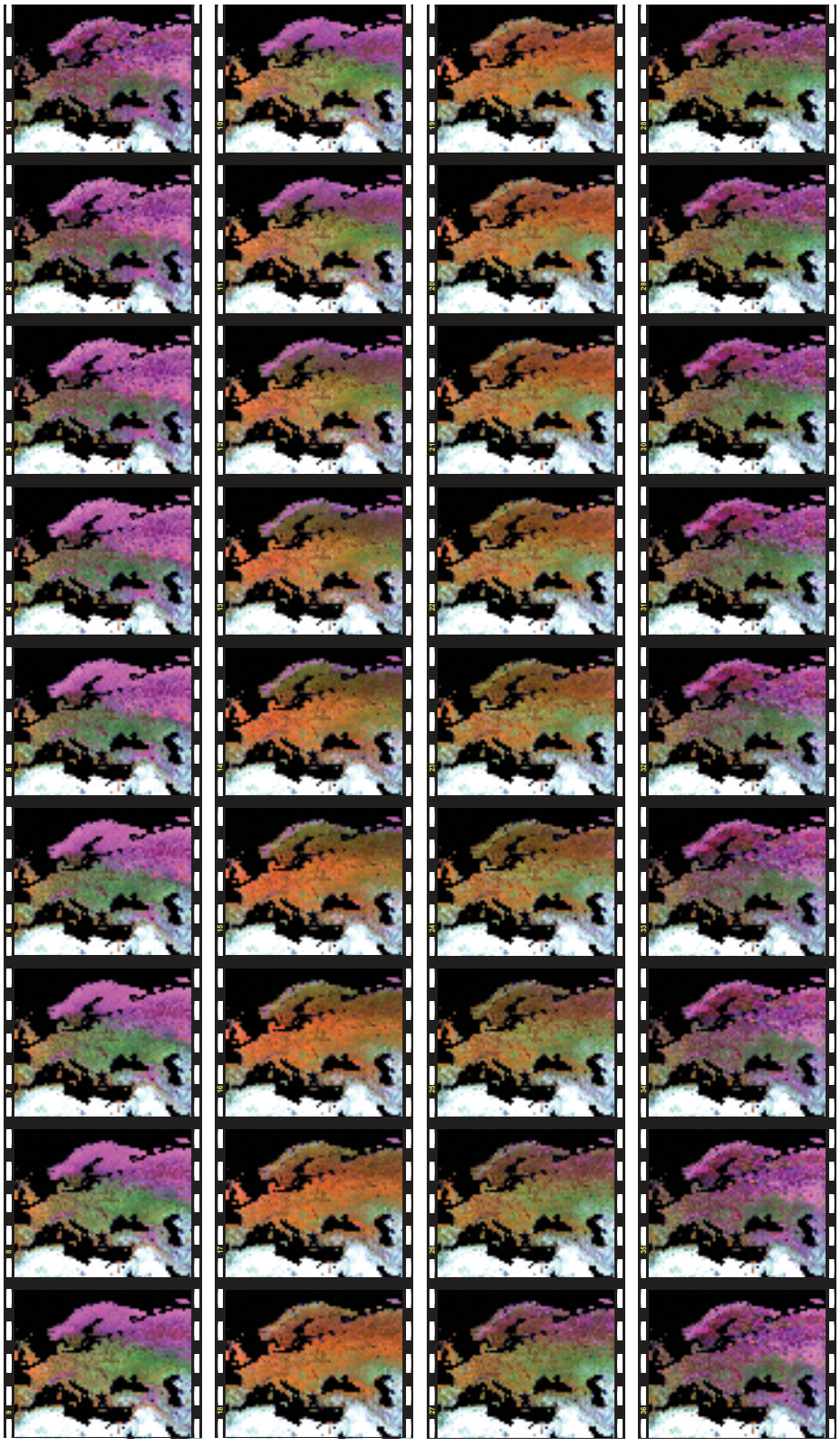

Figure 11.18
Synthesized cloud-free time series of 36 SPOT-VGT images of the year 2002 in the band combination RGB = NIR, SWIR, RED. Each column contains the nine images of each quarter of the year, in chronological order from top to bottom.

11.8 Case study: Flood modelling: Nam Chun (Thailand)

11.8.1 Introduction to case study

In this section we focus a problem that occurs all over the world: flooding. On every continent, floods cause damage and kill people, so one can quite safely say that floods are the most recurring, widespread and disastrous of all natural hazards. The occurrence of most floods is, of course, highly correlated with the meteorological conditions in an area, and since these are difficult to forecast with a high degree of accuracy, it is also difficult to predict flood events. But even if meteorological conditions—especially precipitation—are known, it is no trivial task to forecast floods, let alone to predict their severity. To be able to so, additional information is required, not only regarding the precipitation but also with respect to the area that is likely to be affected. For instance, with precipitation one needs to know the form in which it will fall (rain or snow, ...), the total amount that will fall, its intensity and where exactly it will fall. In short, the precipitation must be spatially-dynamically characterized, where spatial stands for the geographic domain (where) and dynamic for the development over time (when). But also the area that receives the precipitation must be known: what is its size, how steep is it, what is the shape of the watershed that feeds its river system, what are its vegetation and soil characteristics, and how much water is already present to start with? In order to be able to predict how much water will be at a certain place at a certain time, we must enter the world of spatial-dynamic modelling.

Spatial-dynamic modelling

Most GISs have limited dynamic modelling capabilities, especially when it comes to problems where the output of a given time-step becomes the input of the next time-step. In most cases, therefore, a GIS is used in parallel with, i.e. in addition to, a dedicated spatial-dynamic model; the GIS is used to prepare the spatial input data that the model requires and to analyse and further elaborate the model's spatial output (see Figure 11.19). Of course there are exceptions to this, such as the dynamic GIS PCRaster developed by the University of Utrecht and some advanced models that contain basic GIS functionalities. In our case study, we will use, in sequence, two spatial-dynamic models parallel to a GIS. The first model is a rainfall-runoff model that is used to predict discharge at the outlet of a catchment—the upstream part—as a function of the rainfall and the characteristics of the catchment. The discharge predictions become the input for the second model: a 1D/2D hydraulic model that simulates the flow of water over (and through) complex topography in the downstream part of a catchment. It is used to assess the spread of flood water in order to estimate the consequences of flooding in the affected parts downstream.

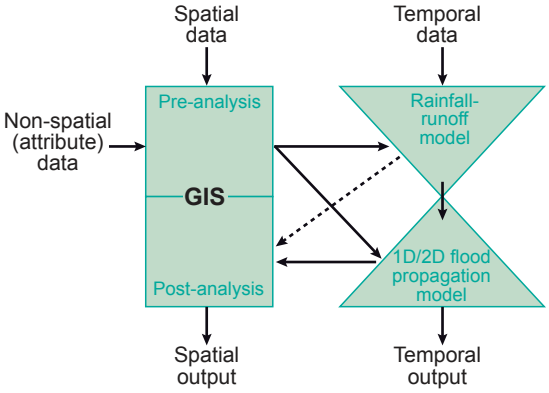

Figure 11.19
Parallel use of GISs and spatial-dynamic models

The Nam Chun study

On 11 August 2001 the typhoon Usagi passed over central Thailand bringing with it intense and prolonged rainfall. This resulted in numerous flash floods and landslides. Approximately 120 people died in this event and over a 1000 people were made homeless. Very quickly people blamed the extensive and uncontrolled deforestation of central Thailand as the main cause of the widespread destruction the typhoon caused. The province of Petchabun in central Thailand—see Figure 11.20—was one of the worst affected areas. The central event in this disaster was the occurrence of a flash flood that originated in the Nam Chun watershed and caused extensive flood damage downstream on the Pa Sak flood plain.

The study described here was carried out to check to what degree had deforestation affected the generation of the flash flood that occurred and to establish to what extent would reforestation be a useful and effective measure for preventing a repetition of such disastrous flooding.

Figure 11.21 shows the main spatial characteristics of the watershed: an upstream, mountainous part (left-hand side), with relatively steep slopes and deeply incised river valleys; and a downstream part (right-hand side) with relatively flat topography, exhibiting a gentle gradient of approximately 1–2% towards the Pa Sak River, to which the Nam Chun River contributes. The area of the upstream and downstream parts of the watershed is in total approximately 92 km^2.

The upper part of the watershed consists of two parallel sub-catchments of a general west-northwest to east-southeast orientation that have their confluence near where the Nam Chun River enters the Pa Sak valley proper. In terms of lithology, the upstream part consists of uplifted Triassic sedimentary rocks, mainly conglomerates, sandstones and shales. The downstream part consists mainly of Quaternary colluvial and alluvial deposits. The vegetation in the upstream part can be characterized by degraded and disturbed forests on the steeper and higher slopes. In the lower parts, farmers have encroached upon the forest to cultivate maize and other food crops such as beans, cabbage and tamarind. A significant part of the upper catchment is covered by fallow grasslands.

Of the downstream part, almost the entire area is used for agriculture: farmers grow rice in the rainy season (May–September) and tobacco, cucumber and maize in the dry season (October–April). Tree crops such as coconuts, mangos and tamarind are also grown there. The average annual rainfall is 1066 mm per year from an annual average of 120 rainy days, which are concentrated in the period May to September. The average maximum temperature is 34 °C (ranging between 37 °C in April and 31 °C in December.

11.8.2 Surface-runoff modelling in the upstream part

In the study, a distributed erosion model was applied to quantify the amount of runoff in the upper catchment and to obtain hydrographs at the outlet into the Pa Sak valley. This model, the Limburg Soil Erosion Model (LISEM), was used because it takes into account the effect of land cover and soil characteristics in a spatial way. This meant that all model parameters could be represented as maps (in raster format), which not only allowed us to assess the consequences of, for example, land cover changes on the shape of the hydrograph, but also to identify where land cover changes would have the most significant effect. This last capability is important because it offers spatial planners a tool for prioritizing areas where mitigation efforts are likely to have the greatest effect. The reader should note that LISEM is a combined hydrological and erosion model, even though the erosion part was not used in this study: LISEM was applied only as a distributed hydrological model.

Figure 11.20
Location of the Nam Chun watershed in North-Central Thailand.

LISEM is a physically-based hydrological and soil erosion model for simulating hydrology and sediment transport during and immediately after a single rainfall event, and it may be applied in catchments of sizes ranging from 1 ha up to approximately 100 km^2. The model, developed by Utrecht University's, Department of Physical Geography, simulates the effects of both current land use and soil conservation measures on surface runoff and sediment transport. LISEM comprises two basic processes: a water part and an erosion part (Figure 11.22). The hydrological processes incorporated in the model are rainfall, interception, surface storage in micro-depressions, infiltration, vertical movement of water in soil, flow over land and channel flow. The model also incorporates the influence on hydrological and soil erosion processes of compaction (including the influence of tractor tracks), small paved roads, field strips and grassed waterways.

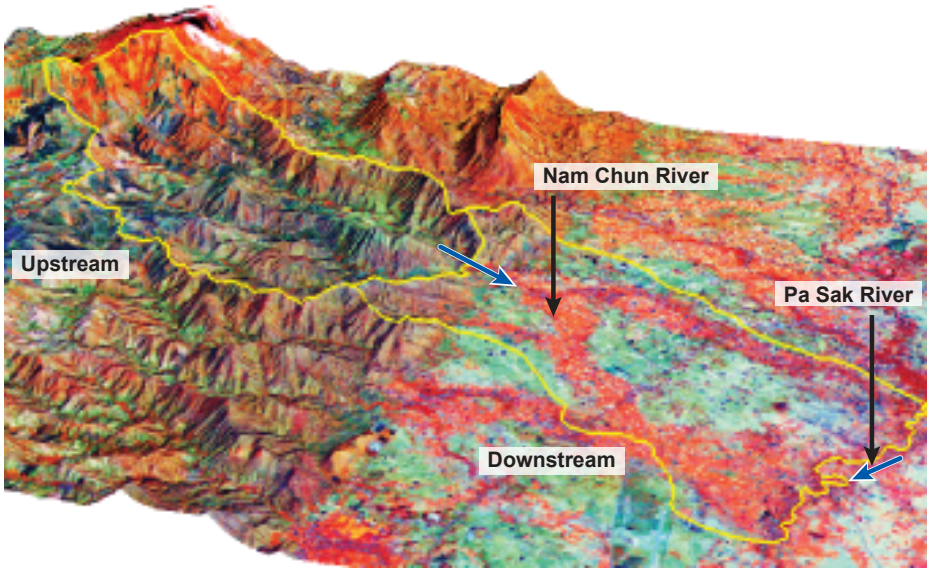

Figure 11.21
A 3D representation of an ASTER false colour composite of the Nam Chun watershed; scale varies in this representation. The view is towards the North.

For the runoff process, rainfall is the basic input. Interception by crops and vegetation is simulated by regarding them as a storage compartment that is to be subtracted from the rainfall. The remaining rainfall then reaches the soil surface, where it can infiltrate or be added to the surface storage. Since LISEM is a storm-based model, the infiltrated water is considered as a loss in the sense that it cannot resurface.

Infiltration can be simulated using one of several available equations, among them those developed by Green & Ampt, Holtan and Richards. In our study we used the Green & Ampt model. Surface storage can be considered as a mini reservoir in which water is stored (think of small ponds and puddles) until a threshold is exceeded. Then overland flow will occur. The flow velocity can be calculated using a combination of Manning's formula and the kinematic wave equation. The flow is directed over the terrain along the local drainage direction, which can be derived from the relevant DTM.

Since LISEM is a process-based model it required a significant amount of input data. All the required input data were derived from three base maps: 1) the digital elevation mode; 2) a soil unit map; and 3) a land cover map. The digital elevation model was derived from the topographic map (Land Development Department, Thailand, based on aerial photographs 1:25,000). The soil unit map was derived from a study by Solomon [107], and values for the infiltration parameters (Ksat) were obtained by Prachansri [93]. A digital land cover map of the study area was produced in 2004 by the Land Development Department of Thailand. The accuracy of the map was found by Prachansri [93] to be 72%, which we considered to be acceptable for the purpose of our study. As LISEM is grid-based, all input maps used in the model were converted into a raster format having a grid size of 30 m $\times$ 30 m. Table 11.2 shows a number of the parameters (collected by Prachansri [93]) required for running the model.

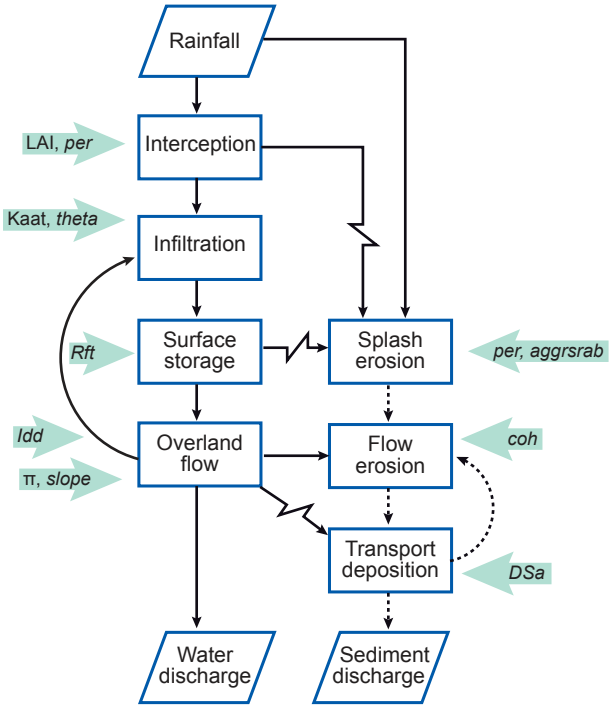

Figure 11.22
Simplified flow chart of the LISEM model.

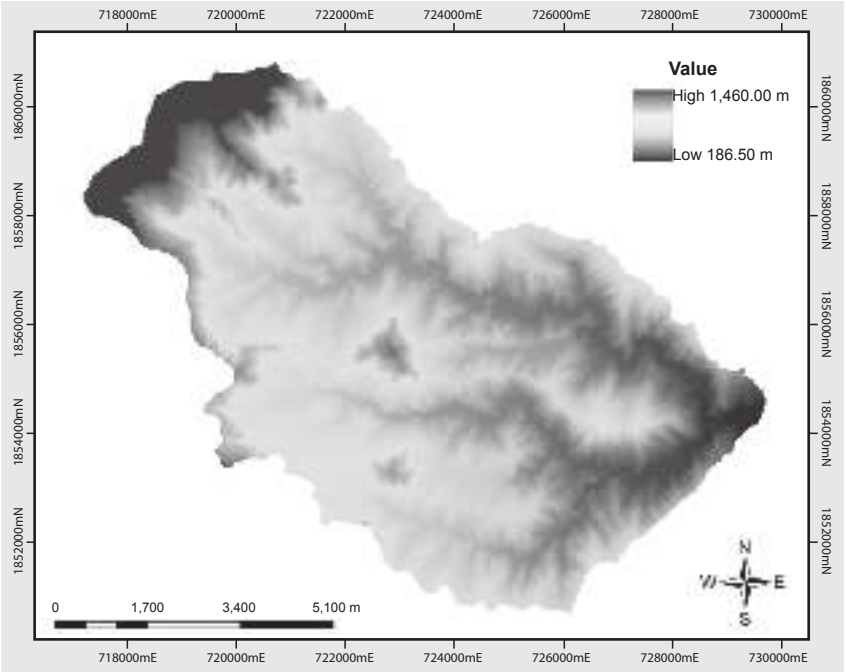

Figure 11.23
Digital Elevation Model (DEM) used in the LISEM model

Table 11.2
Input data for LISEM version 2.39, with the use of the Green & Ampt infiltration model.

Parameter	Name	Method	Unit
Catchment characteristic			
Local drain direction	LDD.map	derived from DEM	-
Catchment boundaries	AREA.map	derived from DEM	-
Area covered by rain gauges	ID.map	field observation	-
Slope gradient (sine of slope angle)	GRAD.map	derived from DEM	-
Location of outlet and sub-outlets	OUTLET.map	derived from DEM	-
Rainfall data	ASCII	field observation	mm/h
Interception			
Fraction of soil covered by vegetation	PER.map	field observation	-
Leaf area index	LAI.map	derived from PER.map	-
Vegetation height	CH.map	field observation	m
Infiltration (Green & Ampt)			
Saturated hydraulic conductivity	KSAT1.map	field measurement	mm/h
Saturated volumetric soil moisture content	THETAS1.map	field measurement	-
Initial volumetric soil moisture content	THETAI1.map	field measurement	-
Soil water tension at the wetting front	PSI1.map	derived from literature	cm
Soil depth	SOILDEP1.map	field observation	mm
Surface storage			
Random roughness	RR.map	derived from literature	cm
Width of impermeable roads	ROADWIDT.map	field observation	m
Overland flow			
Manning's roughness coefficient	N.map	derived from literature	-
Local drain direction of channel network	LDDCHAN.map	derived from ldd.map	-
Channel flow			
Local drain direction of channel network	LDDCHAN.map	derived from ldd.map	-
Channel gradient	CHANGRAD.map	derived from grad.map	-
Manning's *n* for the channel	CHANMAN.map	derived from literature	-
Width of channel scalar	CHANWIDT.map	derived from ldd.map	m
Channel cross-sectional shape	CHANSIDE.map	field observation	-

Model calibration and validation

Many authors have demonstrated the need to calibrate process-based models to achieve acceptable levels of predictive quality. In the case of hydrological models, typically these are calibrated using data measured at the outlet of the relevant catchment. Differences between observations and simulated modelling results can be basically attributed to four different sources of error:

1. errors in the meteorological input data;
2. errors in the recorded hydrological observations;
3. errors and simplifications inherent in the model's structure; and
4. errors resulting from the use of non-optimal parameter values.

During the calibration step, only errors from non-optimal parameter values can be addressed.

In our case study, the results of the LISEM model were evaluated using six selected rainstorm events (Tables 11.7–11.8). Three of these served as a calibration set, to optimize the parameter settings. The other three rainstorms served as a validation set, to test the predictive qualities of the optimized model.

The model results were calibrated primarily on peak discharge, but also on the general shape of the hydrograph. The simulated hydrograph was visually compared with the measured data and the two parameters were used to calibrate on peak discharge:

1. Saturated hydraulic conductivity (Ksat), which determines infiltration rate and amount of runoff; and
2. Surface roughness coefficients. Table 11.3 shows the results for the peak discharge and Figure 11.24 the results for the general shape of the hydrograph. The parameter values obtained after the calibration step can be found in [93].

Events	Rainfall (mm)	Peak discharge ($m^3 s^{-1}$) Observed	Simulated
Calibration			
60905	52.58	37.5	37.90
18095	18.43	13.00	13.40
260905	29.49	31.45	32.99
Validation			
70905	16.60	4.2	4.72
90905	10.61	1.02	1.30
120905	26.74	15.37	23.81

Table 11.3 Observed and simulated peak discharge in the Nam Chun catchment.

Runoff rate for different land cover types

The model enabled us to assess the contribution to runoff from sub-areas within the catchment. The highest volume of surface runoff was predicted for maize cultivations, with an average value of 482×10^{-3} m^3 s^{-1}; the lowest volume predicted was for forest areas, with an average of $13.3 \times 10^{-3} m^3 s^{-1}$. On the whole, agricultural areas, comprising cornfields, mixed crops and orchards, show approximately 16 times higher

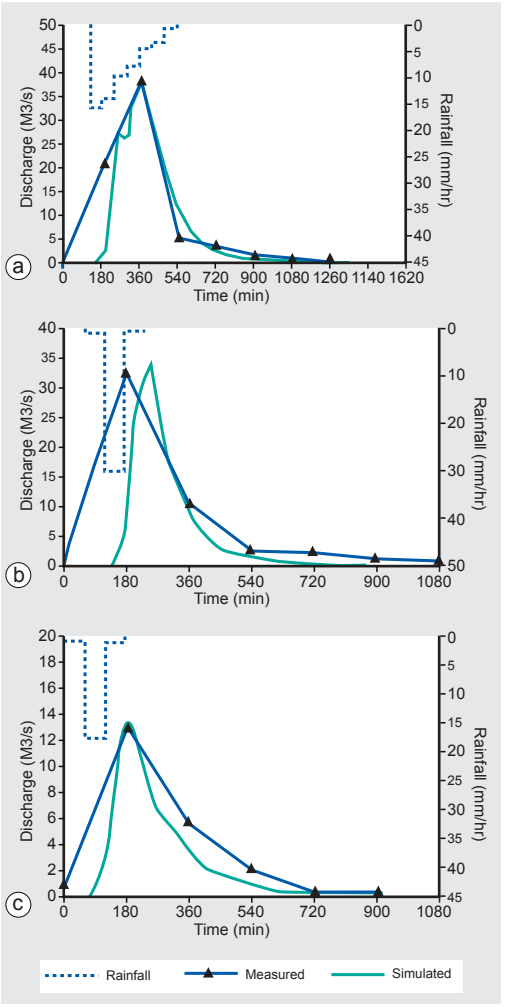

Figure 11.24
Measured and simulated discharge in the Nam Chun catchment on 6 September 2005 (top-left), 18 September 2005 (top-right) and 26 September 2005 (bottom).

rates of surface runoff than non-agricultural areas (comprising forest, degraded forest and grassland areas): 440×10^{-3} m^3 s^{-1} vs. 27.82×10^{-3} m^3 s^{-1} per pixel of 30 m$\times$30 m.

This enormous difference can be attributed to the combination of higher hydraulic conductivity, greater surface cover and higher surface roughness values in the non-agricultural areas, resulting in high infiltration rates, which in effect reduce surface runoff. The spatial and temporal distribution of surface runoff as predicted by the calibrated model is presented in Figure 11.25.

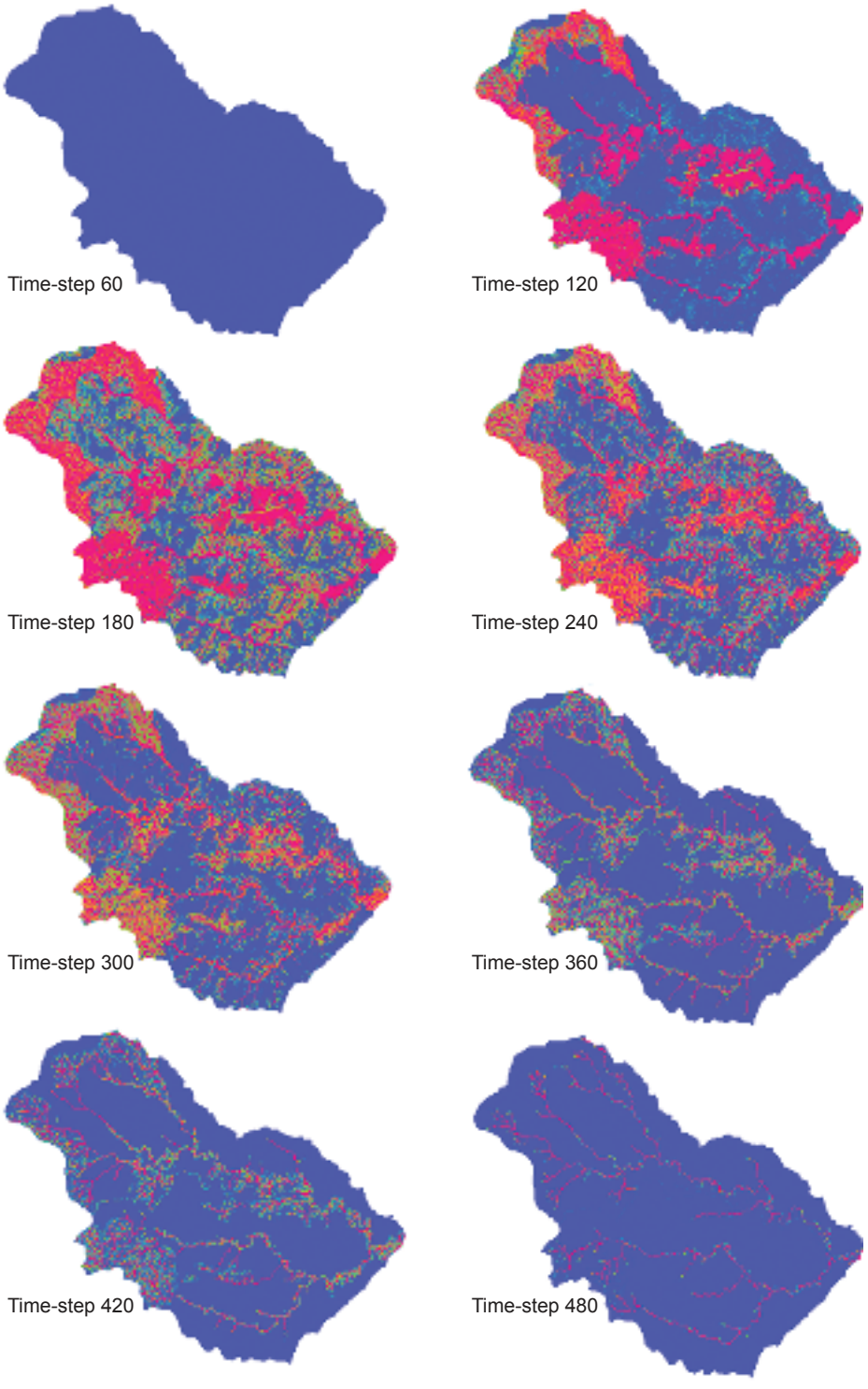

Figure 11.25
Spatial and temporal distribution of surface runoff (time-step = 1 minute).

Scenario generation

Our objective in the Nam Chun study was to evaluate the effects of different land use scenarios on the rate of predicted surface runoff in the catchment. Jetten et al. [49] state that although models may not be able to accurately predict future events, they can be used to compare different scenarios. In scenario studies, the same uncertainty about input data applies to all scenarios and one can, therefore, assume that the differences resulting in the different simulations are in fact a consequence of the scenario changes applied. Therefore, in order to evaluate the effects of different land use scenarios, three land cover scenarios were developed:

- Base scenario: actual situation, i.e. as per August 2001;
- Scenario A: change the entire catchment to forest;
- Scenario B: Change land use to corn cultivation before harvest; and
- Scenario C: Change land use to corn cultivation after harvest (i.e. bare soils).

The results of the scenario simulations are shown in Table 11.4.

Table 11.4
Summary of change in peak runoff and its time of occurrence for a selected event (No. 060905) in relation to different land use scenarios: (A) entire catchment forested; (B) change from forest to corn fields before harvest; (C) change from forest to corn fields after harvest. Change in peak discharge is given compared to that of the actual situation. Peak arrival time for the actual situation was 3.5 h.

Scenarios	Peak discharge(m^3s^{-1})	Change in peak discharge	Peak arrival time difference(h)
Actual situation	37.9		
A	9.3	-76%	+2.0
B	184	+385%	-2.0
C	194	+412%	-3.0

Under Scenarios B and C, total discharge was predicted to increase to approximately 400% compared to that under actual land use (base scenario). This indicates that cultivation of corn increases the amount of surface runoff and that expanding areas of agricultural activity in the watershed will result in a drastic increase in river discharge at the catchment's outlet. Figure 11.26 shows the predicted discharges for the three land use scenarios.

11.8.3 Flood propagation modelling in the downstream part

In previous subsections we have demonstrated how a hydrological model can be used to estimate runoff from a given catchment for various scenarios. In itself this is useful, but in practice it is not in the catchment itself where most flooding problems occur. Flooding is usually greatest on the relatively flat terrain beyond the outlet of the mountainous catchments, where we usually find higher concentrations of human population and property.

In this subsection we demonstrate how to assess the consequences of this runoff in the downstream parts. In order to quantify the effect of upper catchment runoff, a combined 1D/2D hydraulic model was used to model the propagation of the flow over flat terrain. To do this we chose to use the SOBEK modelling suite, which combines one-dimensional channel flow with two-dimensional overland flow.

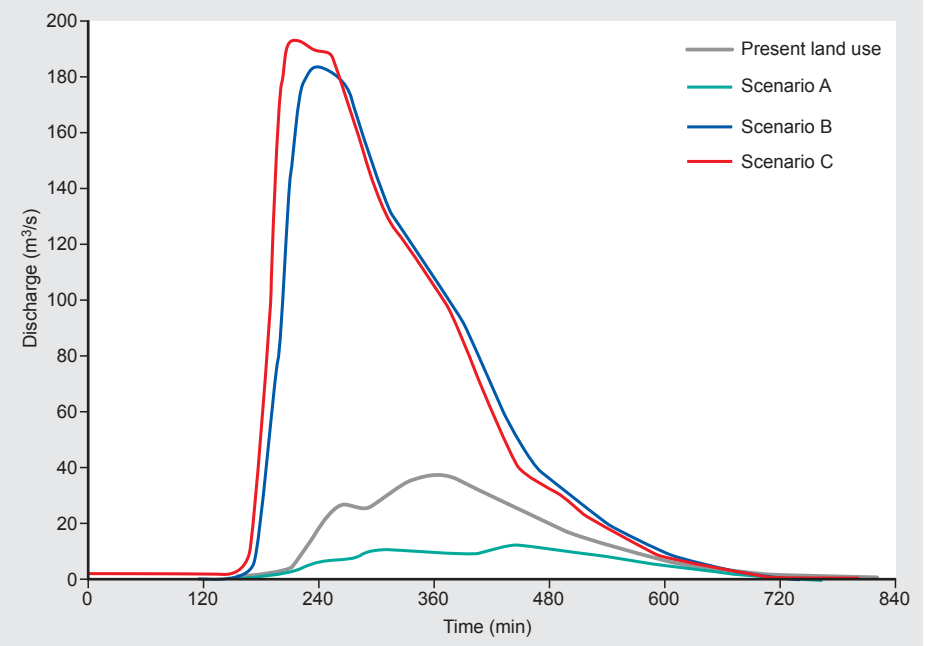

Figure 11.26
Predicted hydrograph for three land use scenarios.

Model data input

Four main types of input data were needed for the model: 1) The digital terrain model, to represent the natural and man-made topography (this includes flow-affecting structures such as embankments and road networks); 2) surface roughness data, to represent the resistance of different vegetation types along the river channel and the flood plain on the water flow; 3) river cross-sections, to represent the shape of the rivers; and 4) the boundary conditions, which include the incoming discharge at the upstream boundary and water levels, or a rating curve, at the downstream boundary. Note that in the model as it was used in this study, there was no direct rainfall in the downstream area: it was assumed that all surface water came from the upstream part of the catchment.

Surface topography

By far the most important input for the model are data that accurately represent the surface topography. Especially for the Nam Chun study, a detailed topographical survey was conducted by the mapping division of the Thai Land Development Department [93], producing 1 m contour lines and spot heights with an accuracy of 0.1 m (Figure 11.27). From this data, a DTM was derived with a grid size of 10×10 m. During a field survey, man-made objects that affect flow, such as embankments, were added to the DTM.

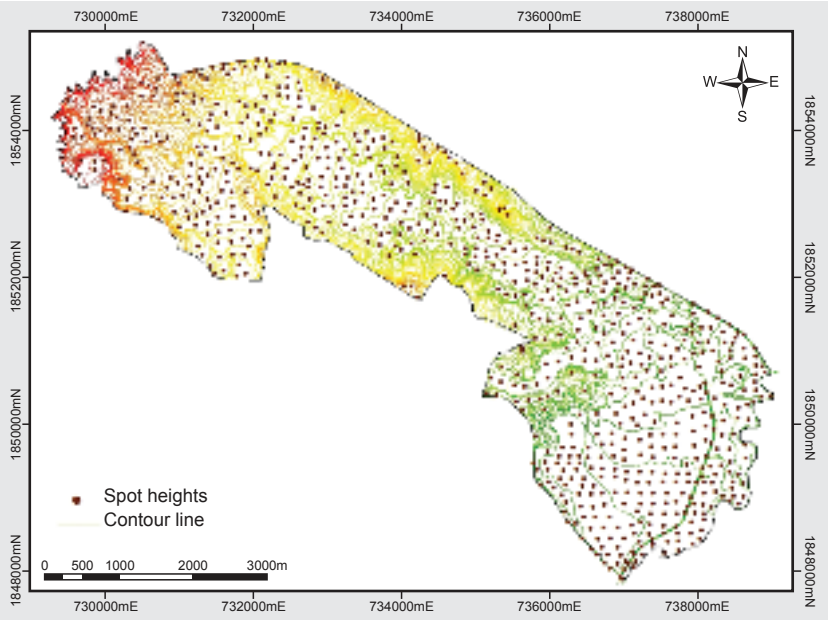

Figure 11.27
Spot heights and contour lines of the Nam Chun flood plain.

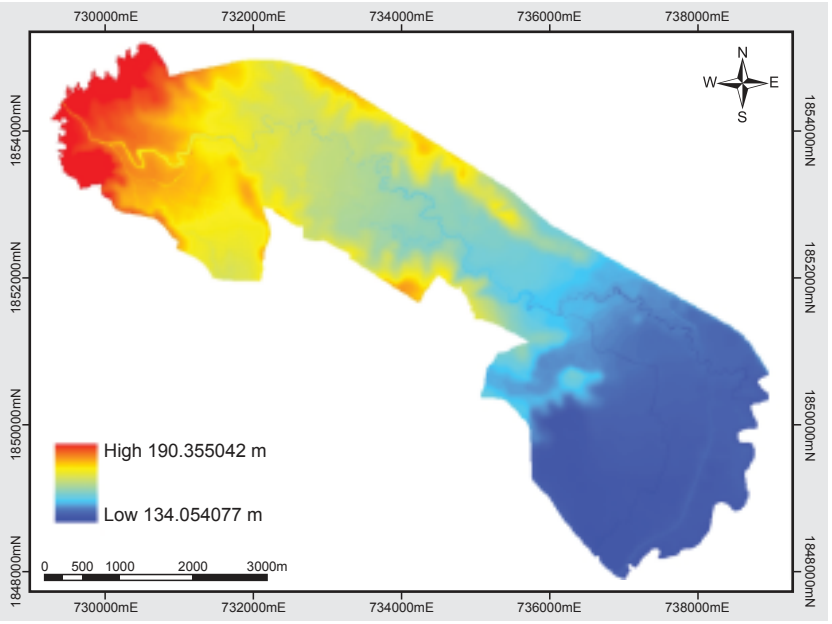

Figure 11.28
Digital Elevation Model of the Nam Chun flood plain.

Surface roughness map

In flood modelling, surface roughness represents the resistance that the water experiences as it flows over the surface of terrain. Surface roughness is strongly related to land cover: smooth, non-vegetated surfaces offer little resistance, whereas dense forests have high friction values. The parameter used for expressing surface roughness is Manning's roughness coefficient. It is hard to measure this coefficient under normal conditions, so usually tabulated values as a function of land cover are used. During calibration procedures, Manning's roughness coefficients are frequently adjusted to improve model performance.

The land cover map that was used for the downstream part of the Nam Chun study was derived using visual interpretation of aerial ortho-photos at a scale of 1:25,000, and the land cover was classified according to the classification standard of Land Development Department of Thailand. The land cover map was further improved during a field survey. The final map is shown in Figure 11.29. This map was transformed into surface roughness values using values of Manning's coefficients taken from the literature; see Table 11.5.

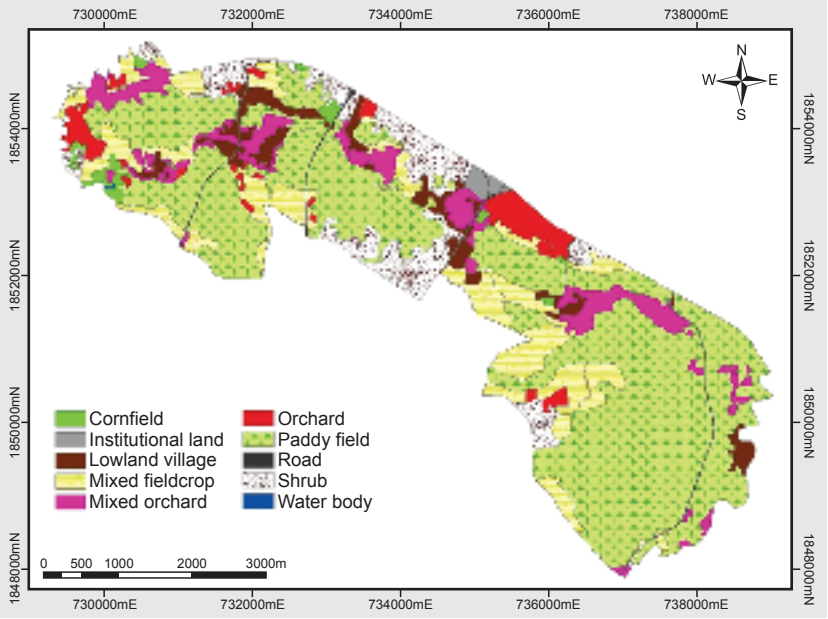

Figure 11.29
Land cover types on the Nam Chun flood plain.

River cross-sections

In this study, cross-section data were derived from the DEM and by surveying during the fieldwork. The channel width and slope of the river bank were measured and visually estimated. River-bed elevations were obtained directly from the DEM.

Boundary conditions

The upstream boundary condition is the discharge prediction from the catchment study as described in Subsection 11.8.2 and Figure 11.26. In our study, not only did we make discharge predictions for the three land use scenarios in the upstream catchment; we also made predictions for rainstorms of different return periods: 2, 10, 20 and 50 years. For example, a rainstorm with a return period of 50 years is an event that, on average, occurs once every 50 years. The return period is a measure of the severity of

Table 11.5
Values of Manning's roughness coefficient for flood plain surface roughness as used in the model.

Land cover types	Manning's coefficient
Cornfield	0.045
Shrub	0.040
Mixed field crop	0.035
Mixed orchard	0.150
Orchard	0.100
Paddy field	0.100
Institutional	0.001
Lowland villages	0.150
Roads	0.001
Water body	0.033

the storm: a longer return period signifies a more severe storm. Hydrographs for all three scenarios are shown in Figure 11.30 a,b. The downstream boundary consists of a time series of water levels observed in the Pa Sak river.

Model output

SOBEK generates several output files, such as maps at predefined time-steps that contain information on water depth and flow velocity; time series of water depth, discharge and flow velocity at predefined locations; and an animation file that shows the progression of the flood. In the Nam Chun study, we used maximum water depths and maximum velocities for the flood-hazard mapping.

Calibration of the model results

In this study, the model was calibrated by comparing water-depth maps with the water depths that were obtained from interviews during fieldwork in 2001, after typhoon Usagi. Unfortunately, there was no information available on the extent of flooding. During the fieldwork, 50 flood-depth points were collected through interviews with the local population. The parameter that was used to minimize differences between the modelling results and observed flood data was the surface roughness coefficient. After a limited number of trials, a set of optimum values was obtained that were used during further analysis. For more information regarding the calibration step, please check [93].

Modelling results for the three land use scenarios

The results shown in Table 11.6 indicate that for a rainstorm with a return period of 2 years under actual land cover the average inundation depth in the upstream part is 0.35 m, although in some places a maximum depth of 0.89 m would be reached. Only 8% of the territory would be flooded in the downstream part (Figure 11.31). Under scenarios in which the upstream catchment is completely transformed into corn fields (Scenarios B and C), the maximum flood-water depth downstream doubles and the spatial extent of flooding on the flood plain more than triples. If the entire upland area is covered by forest (Scenario A), there would be no flooding at all downstream.

Table 11.6
Summary of flooding characteristics under the three land use scenarios for a rainstorm with a 2 year return period.

Total area 25 km^2	Actual situation	Scenario A	Scenario B	Scenario C
Flooded area, km^2	1.92	0.07	7.27	7.65
Total flood volume, $10^6 m^3$	0.29	0.00	2.69	3.20
Average depth, m	0.35	0.14	0.96	0.98
Maximum depth, m	0.89	0.41	2.21	2.25
Maximum velocity, ms^{-1}	1.11	0.12	5.51	5.8

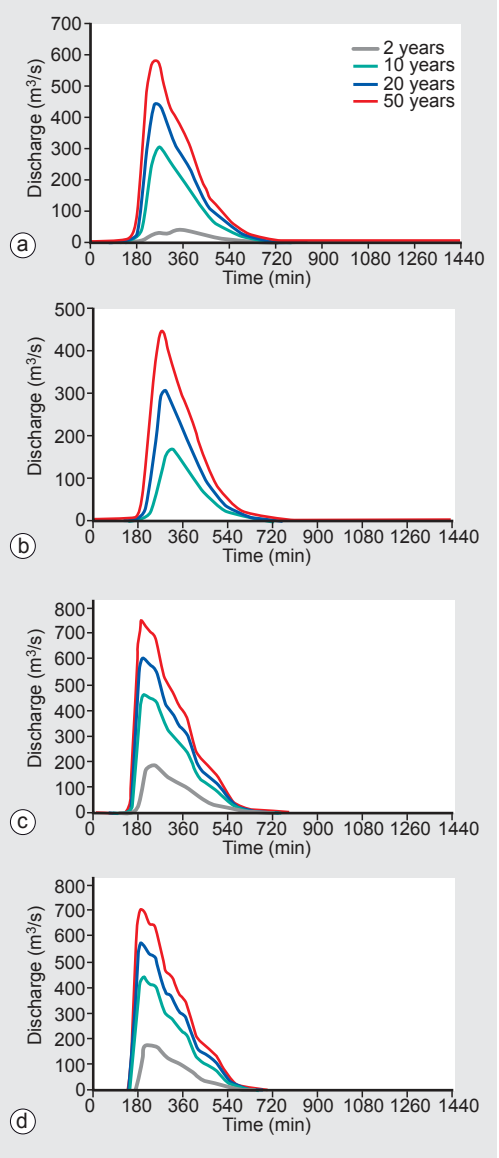

Figure 11.30
Boundary condition for Nam Chun upstream for 4 return periods: (a) actual land use, (b) Scenario A, (c) Scenario B and (d) Scenario C.

11.8.4 Example: flooding following a rainstorm with a 20 year return period

For a rainstorm with a 20 years return period, the results of the model simulation (Table 11.7) indicate that under the actual situation 55% of the area would be inundated. For the Scenarios A, B and C, the inundated area would be 43%, 64%, 63%, respectively. Under Scenario B, the total volume of flood water would be $19.59 \times 10^6 \mathrm{m}^3$, which is twice as high as under the actual situation. For Scenario C, the total of volume of flood water was lower than for Scenario B. This can be explained by the distribution of discharge over time. Under scenario C, for a rainstorm with a 20 year return period (annual probability of occurrence 5%) the discharge is higher at the beginning but after two hours it subsides to levels below that of Scenario B, thus affecting the total volume of the flood water under Scenario B.

Table 11.7
Summary of flooding characteristics under the three land use scenarios for a rainstorm with a 20 year return period.

Total area 25 km^2	Actual situation	Scenario A	Scenario B	Scenario C
Flooded area, km^2	13.87	10.77	16.00	15.77
Total flood volume, 10^6m^3	9.47	5.21	19.59	14.66
Average depth, m	1.53	1.24	1.87	1.79
Maximum depth, m	3.40	2.96	3.90	3.97
Maximum velocity, ms^{-1}	6.04	5.77	6.99	6.92

Maximum water depth

Figure 11.31 and Table 11.8 show that the maximum water depth maps for scenarios B and C are quite similar, with only a small area at the lower part of the map for Scenario B having a greater maximum water depth than for Scenario C. In contrast, the combined maximum water depth class 0.2–1.0 m and flood extent under Scenario C is greater and larger than under Scenario B. These depths are found near the apex of the Nam Chun because under Scenario C the water propagates and inundates in the upper part of the river—then there is less water to drain to the river's lower portion. In Scenario A, the maximum depth of most of the floodwater does not reach 2 m, yet under Scenarios B and C areas of 18% and 9%, respectively, would be flooded by water with depths greater than 2 m; maximum water depths greater than 3 m cover 6% of the surface area under Scenario B. Under Scenario A, 88% of the flooded area has a water depth of less than 1 m.

Table 11.8
Surface area flooded (% of total area) per water depth class for a rainstorm with a 20 year return period.

Water depth, m	actual situation	Scenario A	Scenario B	Scenario C
0 - 0.2	19	28	10	11
0.2 - 0.5	28	33	14	19
0.5 - 1.0	29	27	31	34
1.0 - 2.0	22	11	27	27
2.0 - 3.0	2	1	12	8
$>$ 3.0	0	0	6	1
Total (km^2)	100 (13.87)	100 (10.77)	100 (16.00)	100 (15.77)

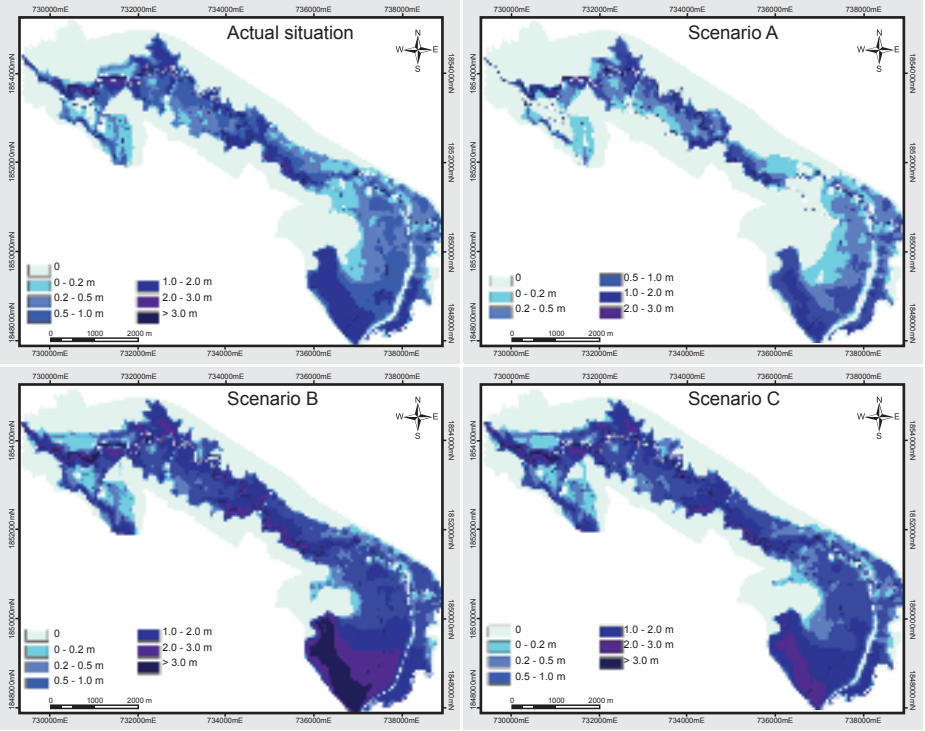

Figure 11.31
The spatial distribution of maximum water depth for the three land use scenarios and actual land use for a rainstorm with a 20 year return period.

Maximum flow velocity

Figure 11.32 and Table 11.9 show the distribution of the maximum flow velocity for the present situation and scenarios A, B and C. For most of the inundated area the maximum flow velocity does not rise above 0.50 m s^{-1}. In scenarios B and C, the maximum velocities of water flow that are less than 0.50 m s^{-1} occur on 97% and 96%, respectively, of flooded area; 4% of the area has a flow velocity greater than 0.50 m s^{-1}. The highest maximum water flow velocities are to be found in the top part of the downstream area (near the apex). In scenario A, for most of inundated area the flow velocity of flood water is lower than 30 cm s^{-1}. This means that if the upland catchment were completely forested, it would reduce the maximum water flow velocity in the downstream area.

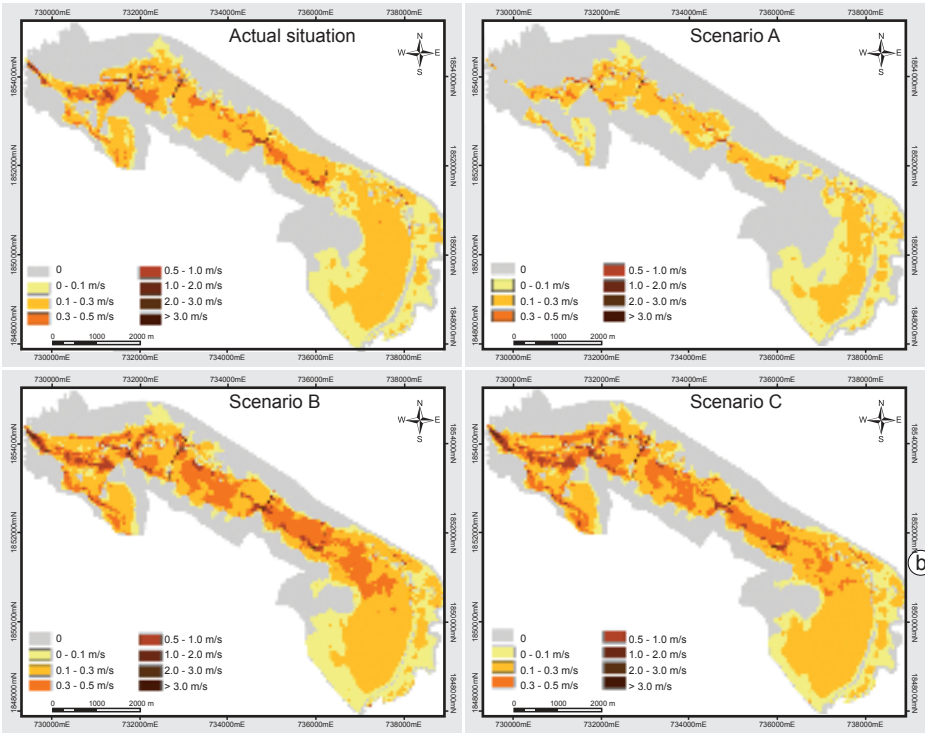

Figure 11.32
The spatial distribution of maximum flow velocity for the three land use scenarios and actual land use for a rainstorm with a 20 year return period.

Table 11.9
Surface area flooded (% of total area) per water velocity class for a rainstorm with a 20 year return period.

Water velocity, ms^{-1}	Actual situation	Scenario A	Scenario B	Scenario C
0 - 0.1	31	50	25	20
0.1 - 0.3	59	47	51	59
0.3 - 0.5	8	3	21	17
0.5 - 1.0	2	0	3	4
1.0 - 2.0	0	0	0	0
2.0 - 3.0	0	0	0	0
$>$ 3.0	0	0	0	0
Total (km^2)	100 (13.87)	100 (10.77)	100 (16.00)	100 (15.77)

11.8.5 Flood-hazard mapping

Flood hazard is the probability of occurrence of a potentially damaging flood event of a certain magnitude within a given time period and area. As part of our case study, we created flood-hazard zone maps from the results of flood modelling simulations for rainstorms with return periods of 2, 10, 20 and 50 years. A different degree of hazard was assigned to each flooding frequency. Five categories of flood hazard were established for each scenario:

- areas with high flood hazard—high frequency of flooding, i.e. a return period of 2 years;
- areas with medium flood hazard—medium frequency of flooding, i.e. a return period of 10 years;
- areas with low flood hazard—low frequency of flooding, i.e. a return period of 20 years;
- areas with very low flood hazard—very low frequency of flooding, i.e. a return period of 50 years;
- areas with no flood hazard.

Figure 11.33 shows the flood hazard zone for each scenario and for the actual situation. A high level of flood hazard that applies to 31% of the area occurs when the whole upstream catchment area is turned over to corn fields (Scenarios B and C). In contrast, the area of high flood hazard becomes smaller if the upstream area is converted to forest. The area of medium levels of flood hazard (for rainstorms of 10 year return period) covers 36% of the terrain in the actual situation and under Scenarios B and C. Under scenario A only 28% of the area has a medium level of flood hazard. The areas of low flood hazard (for rainstorms of 20 year return period) cover only 3, 3, 2 and 1 km^2 under the actual situation, Scenario A, Scenario B and Scenario C, respectively. Thus we can conclude that flood hazard is reduced if the land cover upstream is entirely forest. By contrast, when the upland area is devoted to agriculture, the risk of flooding increases, as does the area of flood hazard.

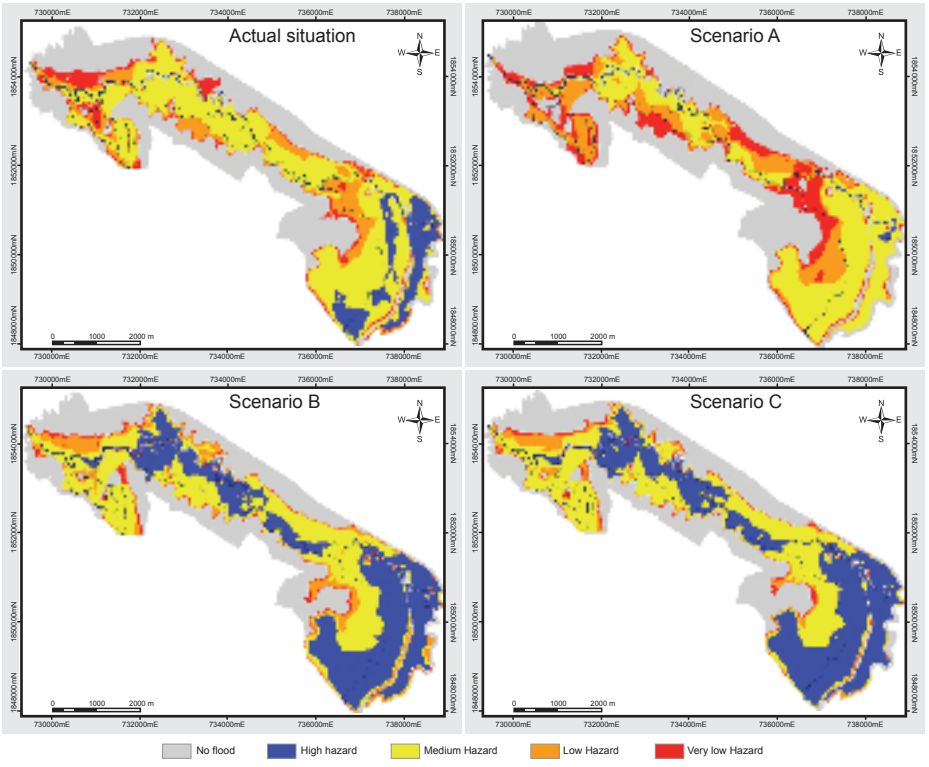

Figure 11.33
Flood-hazard mapping for the three scenarios of land use and actual land use.

11.9 Case study: Environmental management plan for the Lake Uromiyeh ecosystem, Iran

This case study illustrates how data integration at different levels was used in a complex project to support decisions about water allocation in a semi-arid region. The discussion here focuses on data integration issues without going into much detail about the project itself.

11.9.1 Project set up

Lake Uromiyeh (Figure 11.34) lies in the western part of Iran. Its basin covers about 54,000 km^2 and is made up of mountains and river flood plains. The climate is semi-arid, with an average annual rainfall of about 350 mm; low-lying areas (1200–1400 m amsl) receive about 250 mm per year and mountainous areas (around 3000 m amsl) more than 1000 mm, mostly as snow. Irrigated agriculture is the main economic activity in low-lying areas, exploiting both surface water and groundwater resources, while rain-fed agriculture is practised in the foothills of the mountainous areas.

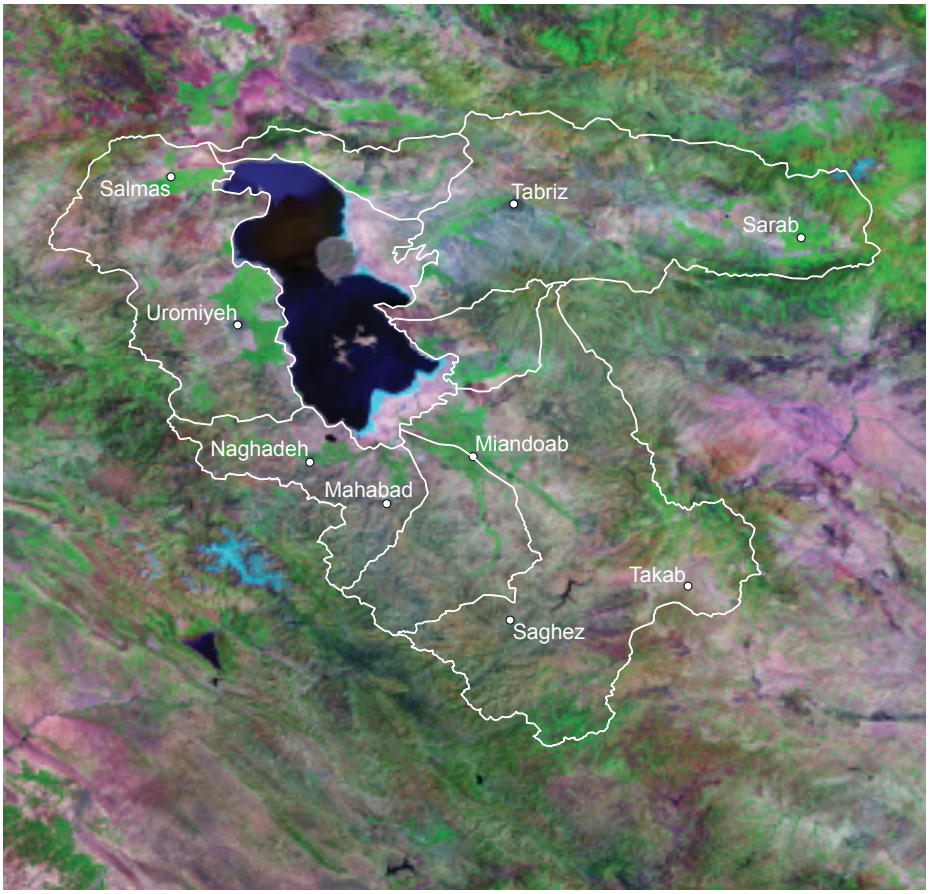

Figure 11.34
Lake Uromiyeh and its watershed; weather stations are sited at locations shown in the basin (source: U.S. Geological Survey Department of the Interior/USGS).

Lake Uromiyeh is shallow (6–8 m deep) and has no outflow, so any precipitation falling in the basin only leaves it through evaporation, either off the land or from the lake itself. The evaporating water leaves behind its dissolved salts, which at the time of the project had resulted in hypersalinity in the lake; the actual salinity depends on the amount of water in the lake, i.e. the lake's water level. These circumstances

have led to the development of a relatively simple ecology with salt-loving organisms populating every level of the food chain.

Falling water levels in the lake caused the shoreline to retreat, leaving behind deserts of salt and resulting in the complete collapse of much of the lake's flora and fauna. These events presented the authorities with a warning that better coordination of water use— involving all stakeholders in the basin—was needed.

The objective of the project was to develop an environmental management plan for the Lake Uromiyeh Basin in the framework of a cooperation between The Netherlands and Iran.

11.9.2 Decision-support system

As the success of the project required the cooperation of all sectors of the economy, as well as all groups of local inhabitants, the concept of integrated water resources management (IWRM) was applied. This entailed the involvement of stakeholders from agriculture, water management, industry, municipalities and water managers, together representing the governmental, private and non-governmental sectors.

The key tool in the integrated management was a decision-support system (DSS) that combined data from all related fields. IWRM, however, involves more than just running a DSS and making decisions on the basis of the outcomes it generates. Rather, it is the process by which the activities of all stakeholders are coordinated. The advantage of using a DSS is that it provides the possibility of testing outcomes of different decision schemes, i.e. of analysing different scenarios.

The DSS for Lake Uromiyeh incorporated a number of software tools, as shown in Figure 11.35.

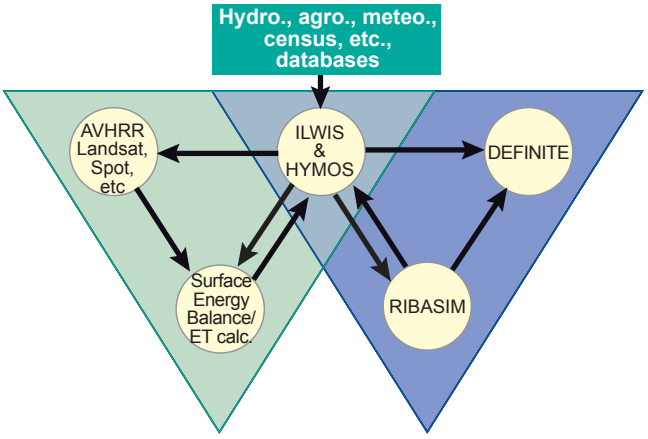

Figure 11.35
Logical structure of the Lake Uromiyeh DSS, indicating the major software tools and data types used.

The DSS comprised four major logical units:

1. external databases (green area in Figure 11.35), which did not form an integral part of the decision-support system;
2. a central spatio-temporal database (purple area) (a loose amalgamation of a GIS and hydrological data management software);
3. EO data and observation models (the overlap area between green and purple areas), which were used independently from the rest of the DSS. (In fact, this part processes input data for the decision support part of the system);

4. process models that exchanged data but were not fully integrated with the central database.

The software tools were not integrated in one computer system, but were used independently. A well-defined data flow scheme represented the logical framework of the DSS.

11.9.3 External databases

Several institutions from different Iranian ministries and departments provided data for the project. Hydrological, agronomic, meteorological, statistical, ecological and topographic data were merged in the central database. In many cases the data were not just copied from the external databases to the DSS: some conversions were made to meet the import requirements of the data storage systems.

11.9.4 Central spatio-temporal database

The central database used was not fully integrated to store the data in a homogeneous manner because the development of such an environment would have exceeded project funding. Instead, efforts were concentrated on storing the data in a practical structure: data for the process models were integrated into a special hydrological data management environment (HYMOS), while the data needed for the EO observation models were stored in an analysis-oriented GIS (ILWIS). This structure is illustrated in Figure 11.36; the special data integration tools and methods are indicated for the relevant steps.

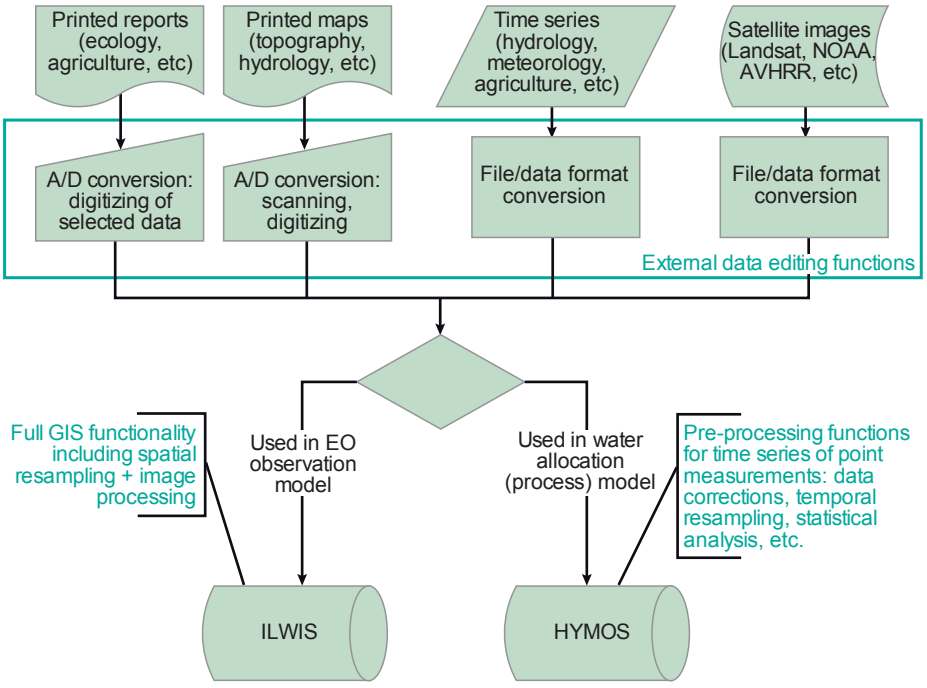

Figure 11.36
Data flows to the central spatio-temporal database of the DSS

An important characteristic of the main units of the central database was the wide range of data processing functions available. ILWIS was used mainly for the spatial operations[1], of which the most frequently used were:

[1]Not all the steps described here were originally carried out during the development phase of the central

- Re-projection of maps. For example, precipitation maps (Figure 11.37) were available originally in geographic coordinates, which were re-projected to the UTM mapping system.
- Spatial re-sampling for adjusting spatial resolution.
  - Re-sampling of coarse resolution to smaller grid size, i.e. densification. Precipitation maps are good examples of this here: the original maps of a course spatial resolution (about 10 km) needed to be densified, since several calculations used a grid of 1 km size. The densification method applied used an interpolation of regularly spaced data.
  - Re-sampling of finer resolution to coarser grid size, i.e. aggregation. This was used for generalizing the land cover/land use map of 28 m resolution that was provided by the Ministry of Agriculture and Jihad of Iran (originally classified from Landsat TM images) to the grid size of 1 km size. To do this a majority filter was used, which assigns the category of highest occurrence within the area of the aggregated cell to the whole cell.
- Spatial interpolation of irregularly-spaced point data; both simple and complex interpolators were used. A typical application was the interpolation of meteorological data (e.g. hours of sunshine) measured at six stations around the basin. For the interpolation, a complex geostatistical method was used that took into consideration both the spatial distribution of the variables shown in the IWMI Water and Climate Atlas of the region and the values actually measured at the stations.

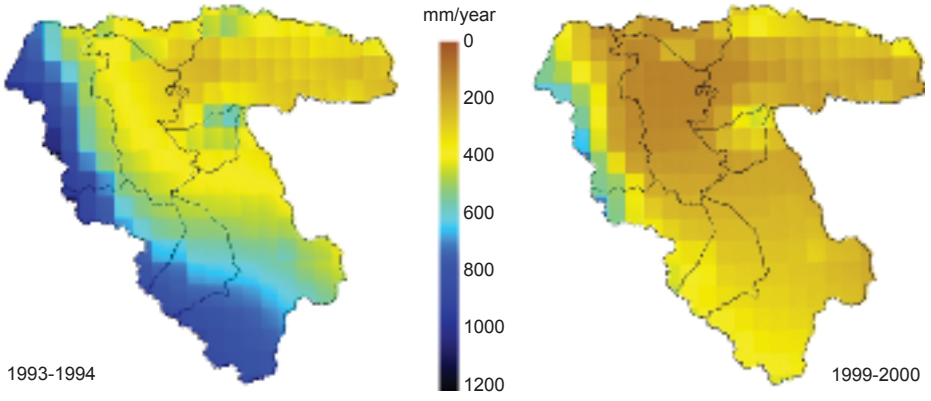

Figure 11.37
Precipitation maps of a wet hydrological year (1993–1994) and a dry hydrological year (1999–2000).

11.9.5 EO data and observation models

Earth observation was an integral part of the data analysis. Two major types of analysis based on Earth observation data were used:

- Satellite images were used for mapping the land cover and defining the major water users from this map (e.g. irrigated and rain-fed agriculture). This is the data flow related to the "Classification" observation model in Figure 11.38. Classification uses statistical methods for creating a link between the observed signal (the image) and the surface properties; the intermediate results were stored in the central spatio-temporal database (not shown in the figure).

spatio-temporal database. In its final form, however, the central database did have capabilities for facilitating these steps.

- A surface energy-balance method (SEBAL) was used for mapping the distribution of the water flux leaving the basin, i.e. evapotranspiration (ET). It is a physically-based (deterministic) model, which uses the relation between the surface physical properties and the electromagnetic energy recorded in the satellite images.

Outputs of the two types of analysis were used to define the water demands of the different sorts of users in a wet (1993/1994) and a dry (1999/2000) hydrological year. The demands calculated were then stored in the HYMOS database.

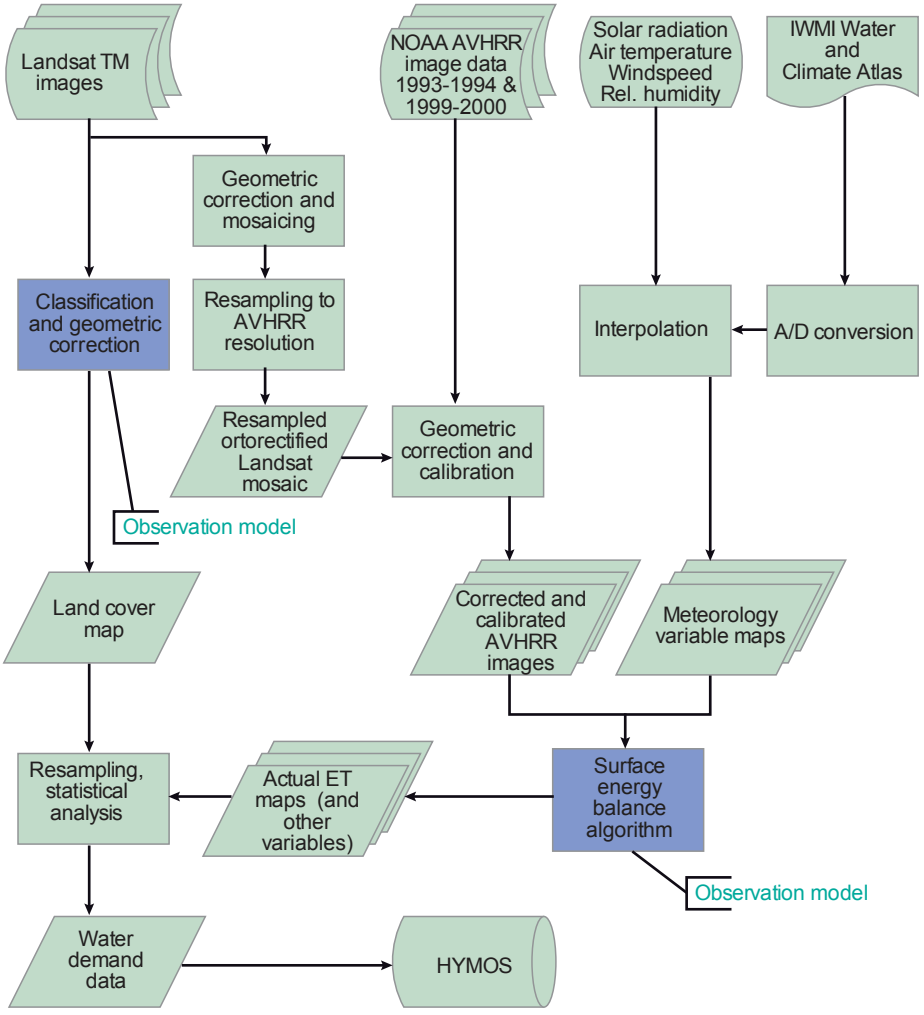

Figure 11.38
Data flows in the EO data and observation models module with a focus on the data integration steps.

11.9.6 Process models

Allocation of water to different users requires a careful evaluation of the water resources available versus the water demands and priorities. The process modelling part of the DSS actually comprised two models:

- The RIBASIM (RIver BAsin SIMulation, developed by Delft Hydraulics) model, which distributes available water resources to users according to priorities and

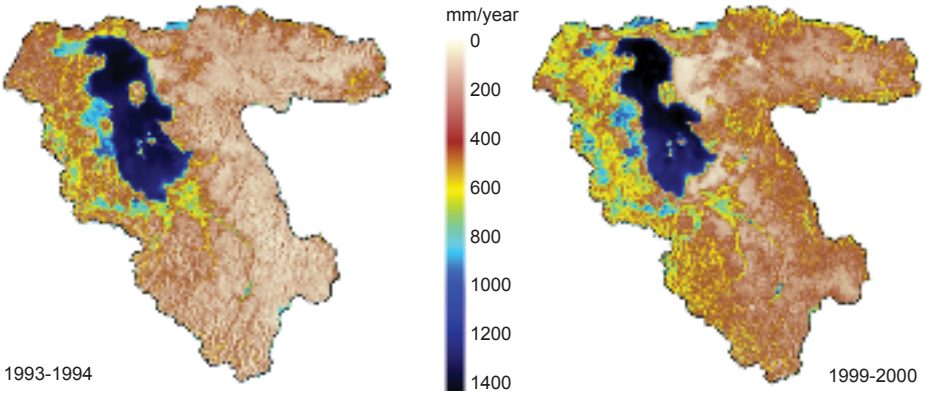

Figure 11.39
Example of the results of the surface energy-balance calculations: actual evapotranspiration maps of the two hydrological years analysed.

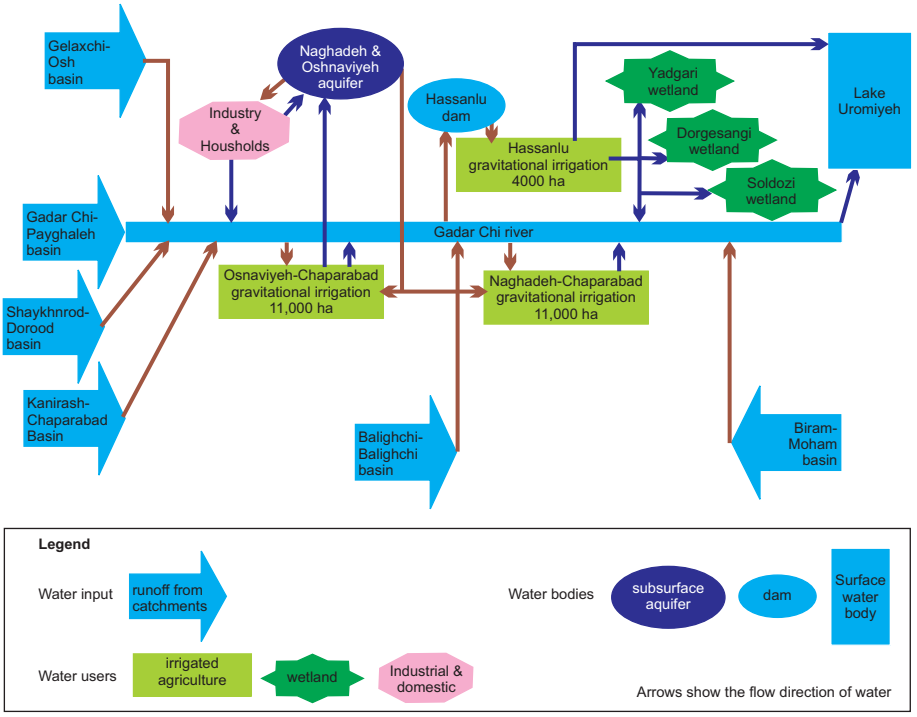

Figure 11.40
Schematic representation of water resources and users in the Ghadar Chai basin: the actual situation.

needs. It is able to simulate the flow of water from the headwaters of rivers to the lowest point of their basins—in our case, from the mountains to Lake Uromiyeh. Water flows can be traced through river channels, lakes, reservoirs and wetlands, as well as groundwater flows from sources to users. The logical structure of the actual situation in one sub-basin (the Ghadar Chai basin) is shown in Figure 11.40. Not only actual situations, but also future scenarios can be simulated with RIBASIM: Figure 11.41 includes four new irrigation schemes, a new dam and a new fish pond. RIBASIM can directly be linked to HYMOS. All the data integration steps are thus made outside the model.

- The DEFNITE (DEcisions on a FINITE Set of Alternatives) model, which is a tool for impact assessment and scenario analysis. A wide range of decision-support tools are included, e.g. multi-criteria methods, as well as tools for cost-benefit

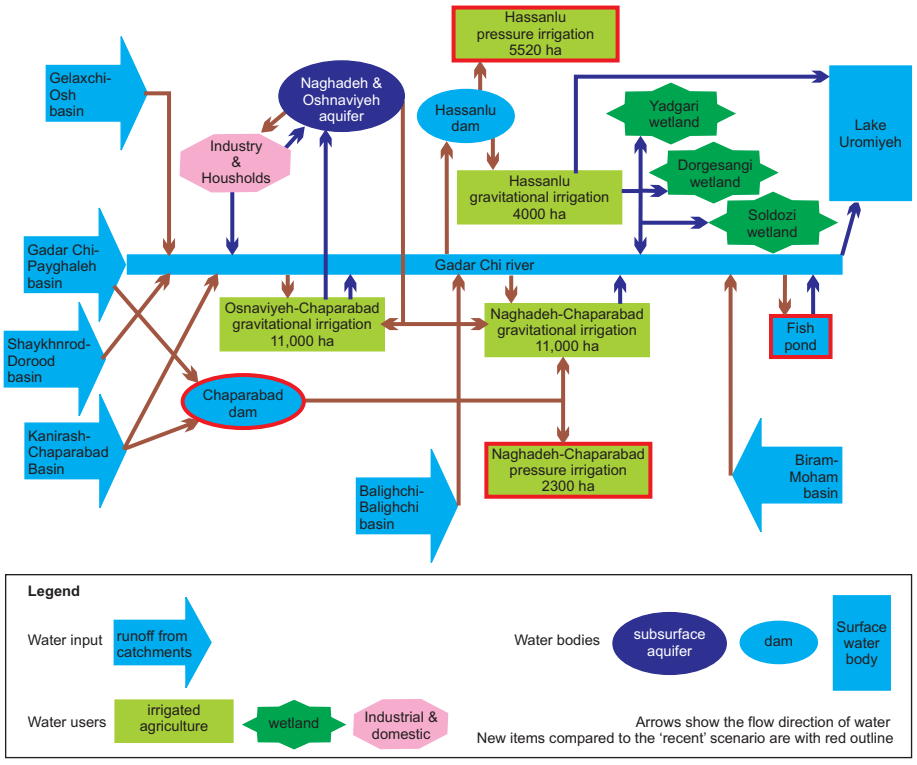

Figure 11.41
Schematic representation of water resources and users in the Ghadar Chai basin: future scenario with extended irrigation schemes.

and cost-effectiveness analyses, are available. For example, DEFNITE can compare different outputs (scenarios) from RIBASIM by assigning weights and assessing the most reasonable option. In this sense, DEFINITE is not a process model itself, but a tool to characterize and analyse the results of process models.

Several scenarios with different priorities and different levels of irrigation development were calculated. The DSS proved that actual water use is, unfortunately, not sustainable. This result poses an enormous challenge for the water managers of the region, especially since demand for water is still rising as a result of increasing social and economic pressures.

11.9.7 Conclusions

Data of different kinds, obtained from several sources, were integrated in the decision-support system developed for the Lake Uromiyeh Environmental Management Plan. The complexity of the situation required various methods of spatial and temporal resampling to create a data set that fitted the analytic methods proposed. Statistical and deterministic observation models were used to calculate the input data for a process model, which provided water allocation scenarios in all the sub-catchments of the Lake Uromiyeh basin. The DSS only supports decisions; it does not make decisions. The modelling results of the study proved that there was a need for new management plans that would match available resources with demand in a sustainable manner.

Acknowledgements

The Lake Uromiyeh project was carried out with the support of the governments of Iran and the Netherlands. The main Iranian contributors were the Water Research In-

stitute; the water, environmental and agricultural authorities in the provinces of East and West Azerbaijan; and Yekom and Pandam consulting companies. Dutch partners included ITC, Deft Hydraulics and Water Watch. As international consultants, Wetlands International and Dr Mike Moser participated in the project.

Chapter 12

Use and Users

Corné van Elzakker
Yola Georgiadou
Thomas Groen
Norman Kerle
Joan Looijen
Andrew Skidmore
Richard Sliuzas
Alexey Voinov
Eduard Westinga

Introduction

Geoinformation systems and information products need to be adjusted to their uses and users. This can be considered as a design process to which we can apply a systematic approach (see Figure 12.1). Who exactly are *users* of spatial information? One view could be that users are those who use a system without the complete technical expertise required to fully understand that system. As most GIS and EO applications are complex, and since almost all maps today are produced by some combination of GISs and EO methods, by this definition virtually anyone who has ever looked at a map is a user: there will be components of the hardware, software, and management or data systems that even an expert is unlikely to fully understand.

At the same time, it would be wrong to think of a user as somebody who sits at the end of the research chain and is only fed information from various flows of observed or derived data. After all, as a recipient of spatial information, the user could have an important role in defining what information should be generated, as well as in what form it should be presented. Moreover, it is often difficult to distinguish the producer of information from the consumer of that information. Perhaps the term stakeholder, which has also been used in the discussion on governance in Chapter 1, is more appropriate, as it connects the use of spatial data and information to an identified issue for which access to and use of spatial data and information are considered to be relevant and important.

It is clear that enormous volumes of data are being generated. This phenomena was identified by the editors of a special 125th anniversary issue of the prestigious science journal *Science* entitled "What we don't know" as a significant scientific challenge.